MINIATURIZED LOOP RESONATOR FILTER USING CAPACITIVELY LOADED TRANSMISSION LINES

MAK HON YEONG

DEPARTMENT OF ELECTRICAL AND
COMPUTER ENGINEERING
NATIONAL UNIVERSITY OF SINGAPORE

2005

MINIATURIZED LOOP RESONATOR FILTER USING CAPACITIVELY LOADED TRANSMISSION LINES

MAK HON YEONG
B.Eng (Hons.), NUS

A THESIS SUBMITTED
FOR THE DEGREE OF MASTERS IN ENGINEERING
DEPARTMENT OF ELECTRICAL AND
COMPUTER ENGINEERING
NATIONAL UNIVERSITY OF SINGAPORE
2005

Table Of Contents

List of Tables

List of Figures

List of Symbols

ε_0	permittivity
μ_0	permeability
λ	wavelength
CTL	capacitively loaded transmission line
TL	transmission line
u_p	phase velocity

Abstract

This thesis details the design and investigation of a miniaturized microstrip closed loop resonator using slow wave structures in the form of capacitively loaded microstrip lines. The primary objective is to achieve resonator and hence filter miniaturization with a secondary objective of achieving improving resonator coupling to aid filter synthesis.

A novel miniaturized closed loop resonator structure that achieves both miniaturization and improved coupling has been developed. The miniaturized resonator is demonstrated to achieve a 37% reduction in area when compared against a square closed loop resonator of equivalent resonant frequency. Also developed are feed structures to provide improved control of external Q_L. To aid resonator design, a methodology to synthesize the new structure based on frequency requirements is provided.

A 3rd order Chebyshev filter using the new resonator structure has been fabricated. In comparison to a filter synthesized using a closed loop resonator of similar size, the new structure achieves a 22% lower resonant frequency and also an additional area reduction of 6% which is possible due to space savings provided by the structure.

Acknowledgements

I would like to thank Professor Leong Mook Seng, Associate Professor Ooi Ban Leong and Doctor Chew Siou Teck for their invaluable advice and guidance to this project. I would also like to thank the staff from the Radio Frequency Laboratory at DSO for providing support for fabrication processes.

Lastly, I would like to thank Mr Ng Tiong Huat and friends at the Microwave Laboratory of NUS for their company and friendship. They have made my academic experience a fulfilling and enriching one.

Chapter 1 : Introduction

1.1 Introduction

The need for miniaturization in modern mobile communication systems has presented new challenges to the design of high performance miniature RF filters and resonators. This is especially so where the frequency of operation falls within L-band (1-2 GHz) and S-band (2-4 GHz).

Microwave resonant structures are used extensively in applications such as filters, oscillators and amplifiers. At low frequencies, resonant structures are realized using lumped elements. At microwave frequencies the use of cavity and microstrip resonators are commonly employed.

A microstrip resonator is any structure that is able to contain at least one oscillating EM field [5]. In general, microstrip resonators can be classified as lump-element or quasi-lumped element resonators and distributed line or patch resonators.

Various methods have been developed to achieve miniaturization, one of which is by exploiting the slow wave effect using capacitively loaded transmission lines (CTL). The CTL concept has been applied in various structures to reduce the size of planar circuits [1] - [3].

This thesis focuses on planar microstrip closed loop resonator and filter design. It proposes the use of CTL to reduce resonator size and concurrently increase coupling between resonators by using stubs to form an interdigital capacitor structure.

1.2 Objectives

The objective of this thesis is to study novel methods to enable miniaturization of microstrip closed loop resonators. The objectives can be listed as follows:

- To develop compact closed loop resonators by using capacitively loaded transmission lines (CTL).
- To develop resonators capable of providing improved coupling performance
- To synthesize filters by using the newly developed resonators

1.3 Scope of Work

The scope of this project can be divided into 3 main portions. The first portion explores the various types of Microstrip resonators.

The second portion looks into slow wave structures and explores how it can be applied to Microstrip closed loop resonators to achieve miniaturisation. A miniaturised closed loop resonator using slow wave structure is developed here. Also developed is a methodology for resonator synthesis.

The third portion explores coupled resonator filter synthesis using the miniaturized closed loop resonator. The new resonator structure is characterized for its design curves such as external Q and coupling coefficient K. Using the characterized information, a third order Chebyshev filter is successfully developed, fabricated and tested.

1.4 Organization

Chapter 2 provides an overview of the types of planar microstrip resonators. A brief description of the different types of microstrip resonators is provided. As the project is focused on closed loop resonators, a common type namely the ring resonators is explored in more detail.

Chapter 3 explores the principle behind slow wave structures and explains how it can be applied to planar microstrip lines in the form of capacitively loaded transmission lines (CTL). A method to synthesize CTL structures is also developed.

Chapter 4 proposes a new class of microstrip closed loop resonators which uses the CTL to achieve resonator miniaturization. The newly synthesized structure is able to achieve 22% reduction in frequency. A method to synthesize the new structure is also developed.

Chapter 5 provides an overview of filter synthesis using arbitrary resonator structures and explains coupled resonator filter synthesis.

Chapter 6 characterizes the external Q and coupling coefficient K of the newly developed resonator structure. Feed structures for coupled line and tapped line coupling are developed for the new resonator structure.

Chapter 7 performs filter synthesis using the newly developed resonator structure. A 3^{rd} order Chebyshev filter of 0.01dB ripple and bandwidth 10% is synthesized here.

Chapter 8 concludes with discussions on the work done and results achieved. Suggestions for future studies are proposed.

1.5 Publications Arising from the Present Work

Based on the works of this research, a paper has been submitted for review and publication in the Microwave and Optical Technology Letters Journal:

H.Y. Mak, S.T. Chew, M.S. Leong, B.L. Ooi, "A Modified Miniaturized Loop Resonator Filter"

Chapter 2 : Microstrip Resonators and Slow Wave Structures

2.1 Introduction

Microwave resonators are used in a variety of applications, including filters, oscillators, frequency meters and tuned amplifiers. [6]

At microwave frequencies, distributed elements are commonly used to achieve resonance. Resonators can be made using microstrip transmission lines, cavities and dielectrics.

2.2 Microstrip Transmission Line

Various forms of planar transmission lines have been developed. Some examples are strip line, Microstrip line, slot line and coplanar waveguide. The Microstrip line is the most popular type and will be described here.

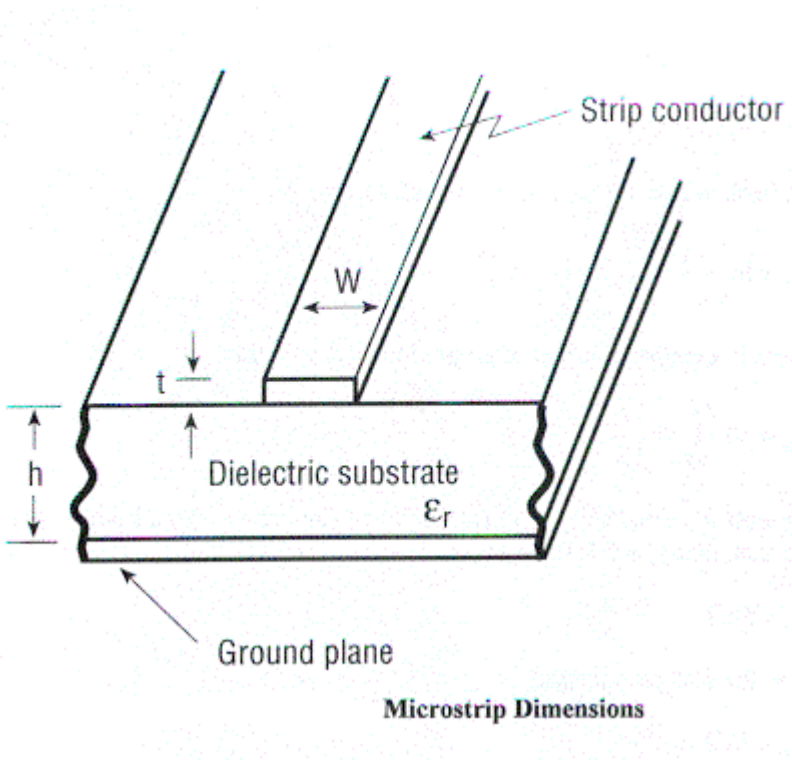

Figure 1: Microstrip Line

The geometry of a Microstrip line is shown Figure 1. A conducting strip of width *W*, thickness *t* lies on the top of a substrate with dielectric constant ε_r and a thickness *h*. At the bottom of the substrate lies a continuous conducting ground plane.

The Microstrip line is an inhomogeneous transmission line. The field between the strip and the ground plane are not contained entirely in the substrate but extends within two media, air and dielectric. Hence the microstrip line cannot support a pure TEM wave. The mode of propagation is quasi-TEM.

The phase velocity and propagation constant can be expressed as

$$u_p = \frac{c}{\sqrt{\varepsilon_e}} \qquad \beta = k_0\sqrt{\varepsilon_e} \quad .$$

The effective dielectric constant of a microstrip line is given approximately by

$$\varepsilon_e = \frac{\varepsilon_r + 1}{2} + \frac{\varepsilon_r - 1}{2}\frac{1}{\sqrt{1 + 12d/W}} \quad .$$

The effective dielectric constant can be interpreted as the dielectric constant of a homogeneous medium that replaces the air and dielectric regions of the microstrip. Given the dimensions of the microstrip line, the characteristic impedance can be calculated as

$$Z_0 = \begin{cases} \dfrac{60}{\sqrt{\varepsilon_e}} \ln\left(\dfrac{8d}{W} + \dfrac{W}{4d}\right) & \text{for W/d} \le 1 \\ \dfrac{120\pi}{\sqrt{\varepsilon_e}\left[W/d + 1.393 + 0.6697\ln\left(W/d + 1.444\right)\right]} & \text{for W/d} \ge 1 \end{cases}$$

For given characteristic impedance Z_0 and dielectric constant ε_r the W/d ratio can be found as

$$\frac{W}{d} = \begin{cases} \dfrac{8e^A}{e^{2A} - 2} & \text{for W/d} < 2 \\ \dfrac{2}{\pi}\left[B - 1 - \ln\left(2B - 1\right) + \dfrac{\varepsilon_r - 1}{2\varepsilon_r}\left[\ln(B - 1) + 0.39 - \dfrac{0.61}{\varepsilon_r}\right]\right] & \text{for W/d} > 2 \end{cases}$$

Where

$$A = \frac{Z_0}{60}\sqrt{\frac{\varepsilon_r + 1}{2}} + \frac{\varepsilon_r - 1}{\varepsilon_r + 1}\left(0.23 + \frac{0.11}{\varepsilon_r}\right) \qquad B = \frac{377\pi}{2Z_0\sqrt{\varepsilon_r}}$$

2.3 Microstrip Resonator

A microstrip resonator is any structure that is able to contain at least one oscillating EM field [5]. There are many forms of microstrip resonators. In general, microstrip resonators for may be classified as lumped element or quasi-lumped element resonators and distributed line or patch resonators. A brief introduction to each of the different resonator types will be explained below.

Lumped or quasi-lumped resonators will oscillate at $f_0 = \frac{1}{2\pi\sqrt{LC}}$.

However they may resonate at other higher frequencies at which their sizes are no longer much smaller than a wavelength. At those frequencies they will no longer behave as lumped or quasi-lumped elements.

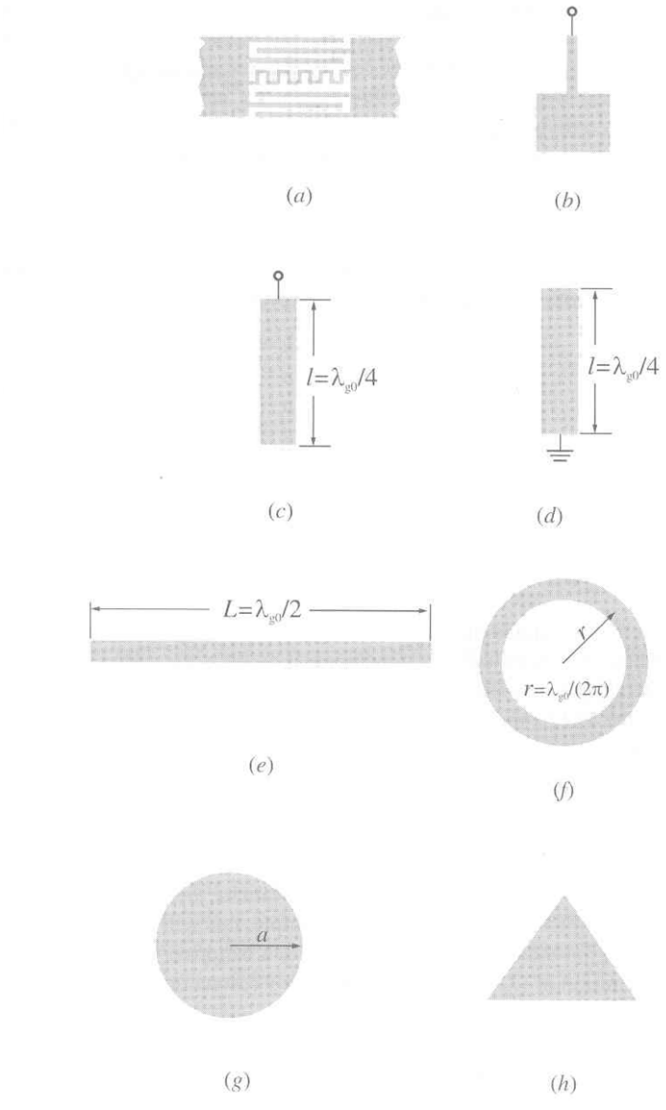

Distributed line resonators are formed by using microstrip lines of various wavelengths ($\frac{\lambda}{4}$, $\frac{\lambda}{2}$, λ) where λ is the guided wavelength at the fundamental resonant frequency f_o.

The quarter wavelength resonator $\frac{\lambda}{4}$ long resonates the fundamental frequency f_0 and at other frequencies of $f = (2n-1) f_0$ for $n = 2,3,\ldots$

The half wavelength resonator $\frac{\lambda}{2}$ long resonates at the fundamental frequency f_0 and at other frequencies of $f = nf_0$ for $n = 2,3,\ldots$ this type of resonator can also be shaped into open-loop resonators.

The full wavelength resonator λ long resonates at the fundamental frequency f_0 and at other frequencies of $f = nf_0$ for $n = 2,3,\ldots$ this type of resonator is commonly found in the form of ring or closed loop resonators with a median circumference $2\pi r = \lambda$, where r is the radius of the ring. Because of its symmetrical geometry a resonance can occur in either of 2 orthogonal coordinates. This type of line resonator has a distinct feature; it can support a pair of degenerate modes that have the same resonant frequencies but orthogonal field distributions. This feature can be utilised to design dual mode filters.

Patch resonators provide increased power handling capability. An associated advantage of patch resonators is their lower conductor losses as compared with narrow microstrip line resonators. Patch resonators usually have a larger size; however, this would not be a problem for applications in which the power handling or low loss is a higher priority.

2.4 Ring Resonator

This project focuses on the development of closed loop resonators. A common closed loop resonator type is the ring resonator. This consists of a transmission line formed in a circular closed loop. The basic ring resonator circuit consists of feed lines, coupling gaps, and the resonator (Figure 2). Power is coupled into and out of the resonator through feed lines and coupling gaps.

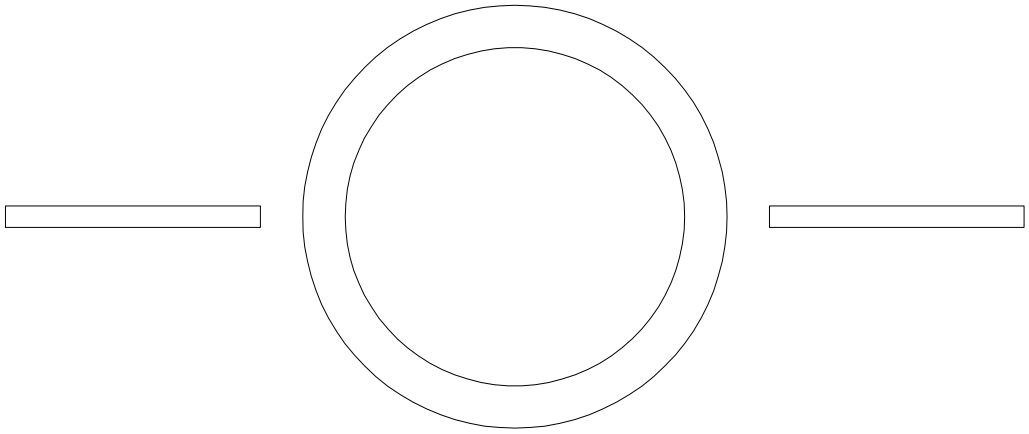

Figure 2: Ring resonator

The ring resonator is a full wavelength resonator λ long. It resonates when the mean circumference of the ring resonator is equal to an integral multiple of a guided wavelength. This may be expressed as

$$2\pi r = n\lambda_g, \quad \text{for n=1,2,3,...} \qquad f = \frac{nc}{2\pi r\sqrt{\varepsilon_{eff}}} = nf_0$$

where $\lambda_g = \dfrac{c}{f\sqrt{\varepsilon_{eff}}}$

and r is the mean radius of the ring that equals the average of the outer and inner radii. λ_g is the guided wavelength and n is the mode number. For the first mode, the maxima of field occur at the coupling gap locations and nulls occur 90^o from the coupling gap locations. This relationship is only valid for the loose or weakly coupled case, as it does not account for loading effects from the ports. [9]

Coupling is said to be weak or “loosely coupled” if the distance between the feed lines and the resonator is large enough such that the resonant frequency of the ring is not affected. If the feed lines are moved closer to the resonator, the gap capacitance increases. If capacitance is sufficiently large, resonator loading will occur and may cause the resonant frequency of the circuit to deviate from the intrinsic resonant frequencies of the ring. Hence when measuring a resonator, the capacitance of the coupling gaps has to be considered.

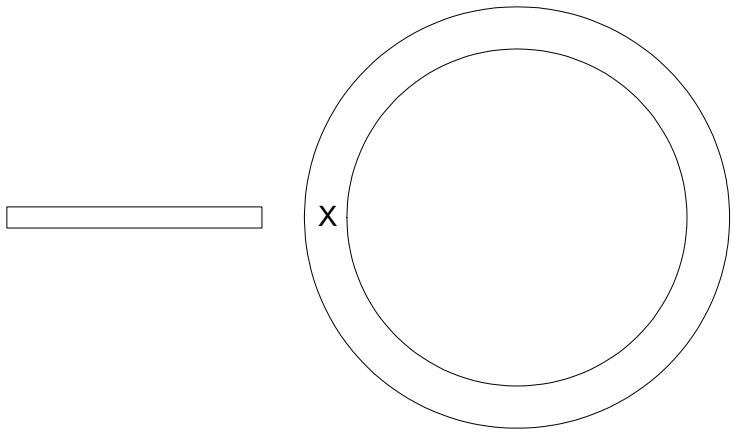

Figure 3: ring resonator with one feed line

The ring can be fed by using only one feed line Figure 3. This configuration is used in dielectric constant, Q-measurements and ring stabilised oscillations. In this configuration for the first mode, maximum field occurs at the coupling gap however a minimum occurs at the opposite side 180^{o} from the coupling gap. Hence when fed using a single feed, the ring behaves as a half wavelength resonator. Resonance occurs when the ring circumference is equals half of a guide wavelength:

$$2\pi r = n\frac{\lambda_g}{2}, \quad \text{for n=1,2,3,...} \qquad\qquad f = \frac{nc}{4\pi r\sqrt{\varepsilon_{eff}}} \ .$$

2.4.1 Ring Equivalent Circuit and Input Impedance

The ring resonator Figure 2 can be modelled by a lumped-parameter equivalent circuit in the form a 2-port network Figure 4. The circuit can be reduced to a 1-port circuit by terminating one of the ports with arbitrary impedance. The terminating impedance should correspond with the feed impedance, which is usually 50 ohms. [11]

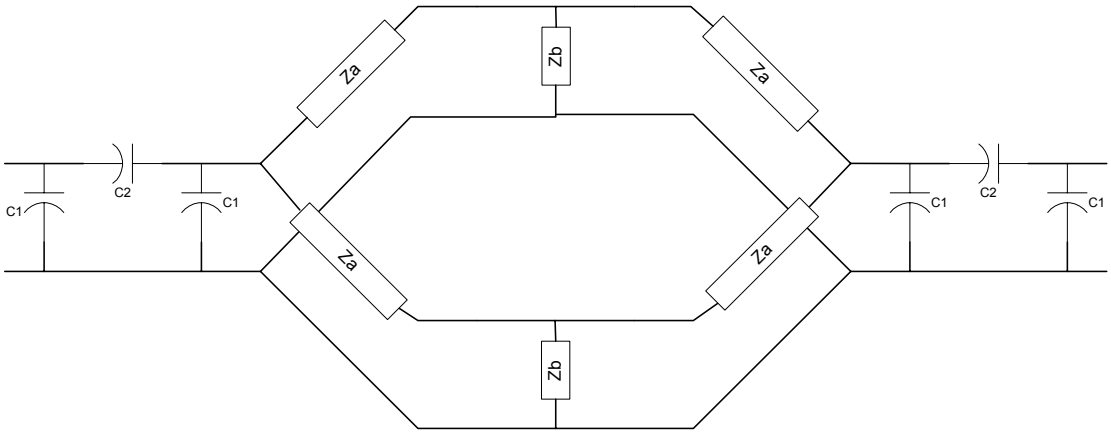

Figure 4: Equivalent circuit of ring resonator

Because of symmetry of the circuit, the input impedance can be found by simplifying parallel and series combinations. The input impedance is expressed as:

$$R_{in} = \frac{C\left(C_1 + C_2\right)\left[\left(C_1 + C_2\right) - \omega D\left(C_1^2 + 2C_1C_2\right)\right]}{\left[\left(C_1 + C_2\right) - \omega D\left(C_1^2 + 2C_1C_2\right)\right]^2 + \left[\omega C\left(C_1^2 + 2C_1C_2\right)\right]^2}$$

$$+ \frac{\left[D\left(C_1 + C_2\right) - \omega^{-1}\right]\left[\omega C\left(C_1^2 + 2C_1C_2\right)\right]}{\left[\left(C_1 + C_2\right) - \omega D\left(C_1^2 + 2C_1C_2\right)\right]^2 + \left[\omega C\left(C_1^2 + 2C_1C_2\right)\right]^2}$$

$$X_{in} = \frac{\left[D\left(C_1 + C_2\right) - \omega^{-1}\right]\left[\left(C_1 + C_2\right) - \omega D\left(C_1^2 + 2C_1C_2\right)\right]}{\left[\left(C_1 + C_2\right) - \omega D\left(C_1^2 + 2C_1C_2\right)\right]^2 + \left[\omega C\left(C_1^2 + 2C_1C_2\right)\right]^2}$$

$$+ \frac{\left[D\left(C_1 + C_2\right) - \omega C^2\left(C_1 + C_2\right)\left(C_1^2 + 2C_1C_2\right)\right]}{\left[\left(C_1 + C_2\right) - \omega D\left(C_1^2 + 2C_1C_2\right)\right]^2 + \left[\omega C\left(C_1^2 + 2C_1C_2\right)\right]^2}$$

where

$$C = \frac{AZ_b^2}{(2A)^2 + \left(Z_a - 2B - Z_b\right)^2}$$

$$D = \frac{1}{2}\left[\left(Z_a - Z_b\right) - \frac{Z_b^2\left(Z_a - 2B - Z_b\right)}{\left(2A\right)^2 + \left(Z_a - 2B - Z_b\right)^2}\right]$$

$$A = \frac{RC_2^2}{\left(C_1 + C_2\right)^2 + \left[\omega R\left(C_1^2 + 2C_1C_2\right)\right]^2}$$

$$B = \frac{\left(C_1 + C_2\right) + \omega^2 R^2\left(C_1^2 + 2C_1C_2\right)\left(C_1 + C_2\right)}{\omega\left(C_1 + C_2\right)^2 + \omega\left[\omega R\left(C_1^2 + 2C_1C_2\right)\right]^2}$$

where R is the terminated load,

and the input impedance is $Z_{in} = R_{in} + jX_{in}$

Resonant occurs when X_{in}=0.

2.4.2 Modes, Perturbations, and Coupling Methods of Ring Resonators

The ring resonator supports various different modes. The modes excited in the annular ring element can be controlled by adjusting the excitation and perturbation. Resonant modes are divided into groups according to types of excitation and perturbation. They are the:

1) Regular mode, and
2) Forced mode

Regular resonant modes

A regular mode is obtained by applying symmetric input and output feedlines on the annular ring element. The resonant wavelengths of the regular mode are determined by $2\pi r = n\lambda_g$.[9]

The ring can be analysed as 2 half-wavelength linear resonators connected in parallel. The parallel connection removes problems related to radiation from open ends hence enabling a higher Q compared to linear resonator.

Resonance occurs when standing waves are setup in the ring, this happens when circumference is integer multiple of guided wavelength. In the absence of gaps or other discontinuities, maximum field occurs at the position where the feed line excites the resonator. The number of maximum field points increases with the mode order as shown in Figure 5.

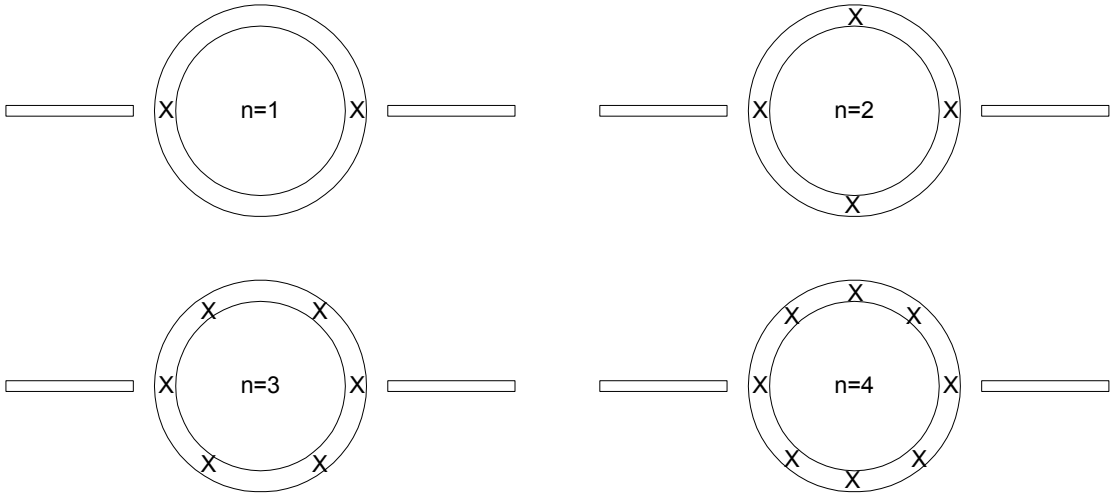

Figure 5: Maximum field points for different resonant modes

Forced Resonant Modes

Forced modes are excited by forced boundary conditions on a microstrip annular ring element. The boundary condition can either be open or short. The open boundary condition is realised by cutting slits on the annular ring element. The shorted boundary condition is realised by inserting vias to ground inside substrate. This forces minima of electric field to occur on both sides of the shorted plane.

With the boundary conditions determined, the standing wave pattern and hence maximum field points inside the ring can be determined.

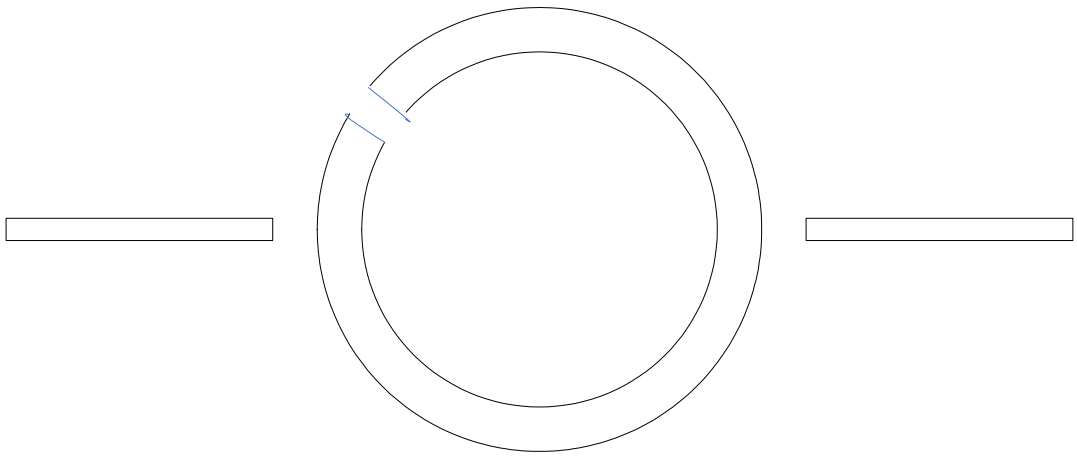

Figure 6: Ring resonator with slit

2.4.3 Applications Using Ring Resonators

The microstrip ring resonator is applied in many different applications such as for measurement applications, filters, couplers, magic-T circuits and antennas. A brief summary of the many different applications for ring resonators are given below:

1) Measurement: Dispersion , dielectric constant ,
   Q measurement and discontinuity measurements
2) Filter: bandpass filters, dual-mode bandpass filters,
   Slotline ring filters
3) Ring couplers: 180° Rat-race hybrid ring couplers,
   180° reverse phase back to back baluns,
   180° reverse phase hybrid ring couplers,
   90° branch line couplers
4) Ring Magic-T Circuits: 180° double-sided slotline ring magic T
5) Ring Antennas: Slotline ring antennas,
   Dual frequency ring antennas

2.5 Slow Wave Structures

This sub-section explains the principle behind slow wave structures and how they can be applied to Microstrip lines. First the Lossless transmission line will be explained. Following that, the Capacitively Loaded Transmission line (CTL) will be introduced.

2.5.1 Lossless Transmission Line

A physically smooth and lossless transmission line (TL) is characterized by the following parameters:

Characteristic Impedance:

$$Z_0 = \sqrt{\frac{L}{C}}$$

Phase velocity:

$$u_p = \frac{1}{\sqrt{LC}} = \frac{1}{\sqrt{\mu \epsilon_e}} = \text{constant depending on medium}$$

where

$$L = \frac{Z_0}{u_p}, \quad C = \frac{1}{u_p Z_0}$$

Since $LC = \mu\varepsilon_e$ therefore for a given dielectric constant ε_r, it is not possible to reduce u_p by increasing inductance or capacitance per unit length because an increase in inductance L leads to a decrease in capacitance C. $\uparrow L \Longleftrightarrow \downarrow C$

Hence for a physically smooth transmission line, reduction in phase velocity u_p is only possible by increasing ε_r [4].

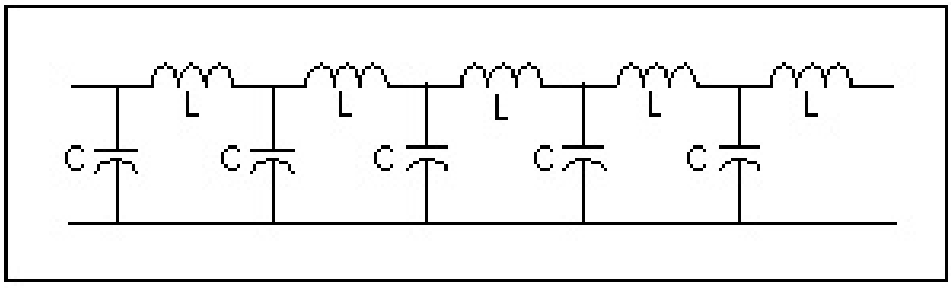

Figure 7: Lossless transmission line circuit

2.5.2 Capacitive Loaded Transmission Lines (CTL)

By removing the restriction that the line should be physically smooth, an effective increase in the shunt capacitance per unit length C can be achieved without a decrease in inductance L [4]. This is achieved by loading a transmission line with shunt capacitance C_p at periodic intervals d.

Here, the CTL is formed by loading a microstripline with shunt capacitance created using open stubs at periodic intervals which are much shorter than the guide wavelength as shown in Figure 8. This causes the periodic structure to exhibit slow wave characteristics.

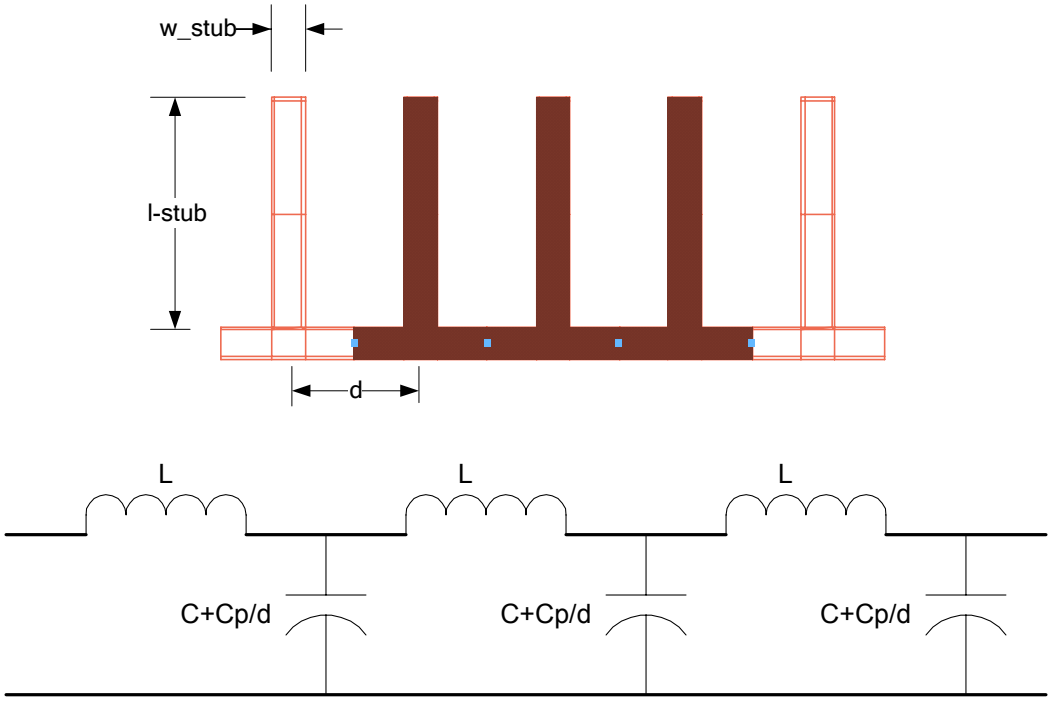

Figure 8: Capacitively loaded transmission line

The effective characteristic impedance and phase velocity of the CTL are given by the following equations:

$$Z_{0CTL} = \sqrt{\frac{L}{C + \frac{C_p}{d}}} \qquad (\Omega)$$

Where $\frac{C_p}{d}$ = lumped capacitance per unit length

$$u_{pCTL} = \frac{1}{\sqrt{L(C + \frac{C_p}{d})}} \qquad (\text{ms}^{-1})$$

$$= \left(\sqrt{\frac{Z_0}{u_p}\left(\frac{1}{u_p Z_0} + \frac{C_p}{d} \right)} \right)^{-1}$$

$$= \left(\sqrt{\frac{1}{u_p^2} + \frac{Z_0 C_p}{u_p d}}) \right)^{-1}$$

For an N section CTL, its electrical length is given by:

$$\phi_{CTL} = \frac{Nd\omega_0}{u_{pCTL}} = Nd\omega_0 \sqrt{L\left(C + \frac{C_p}{d} \right)} \qquad \text{(rad)}$$

where ω_0 is the frequency of interest.

The loaded capacitance of a unit cell is given by:

$$C_p = \frac{\phi_{CTL}\left(Z_0^2 - Z_{CTL}^2 \right)}{n\omega Z_0^2 Z_{CTL}} \qquad (\text{F})$$

The above equations show that to reduce CTL phase velocity u_{pCTL}, either one or a combination of the following methods may be used:

1. Increase the characteristic impedance of the unloaded unit cell Z_0 this is achieved by reducing the microstripline width W_{TL}
2. Reduce the distance between stubs d

3. Increase the loaded capacitance C_p, this is achieved by controlling the following stub parameters:

   For an open circuit stub, $Z_{oc} = \frac{Z_{stub}}{j\tan[\beta\ell]} = \frac{1}{j\omega C_p}$

   $$\omega C_p = \frac{\tan[\beta\ell]}{Z_{stub}}$$

   Where C_p can be increase by:

   a) increasing the stub electrical length $\beta\ell \to \frac{\pi}{2}$

   b) Reducing the stub characteristic impedance $\downarrow Z_{stub}$. This is achieved by increasing the width of the stub $\uparrow W_{stub}$

The effects of varying these parameters can be verified with ADS circuit simulation. A demonstration of the effects of varying CTL parameters is also shown in section 3.3.1.

Chapter 3 : Closed Loop Resonator Miniaturisation

3.1 Introduction

Microstrip closed loop resonators are commonly used for applications such as filters, measurement of dielectrics, couplers, magic-T circuits and antennas. However its large physical size can present a drawback. Hence there is strong interest to miniaturize such resonators particularly for filter applications.

Miniaturization of microstrip filters and resonators may be achieved by using high dielectric constant substrates or lumped elements, but very often for specified substrates, a change in the geometry of filters is required and therefore new filter configurations become possible. One of the ways in which resonator size can be miniaturised without a change in substrate is by meandering the lines to create a folded microstrip resonator [10].

Various methods that have been explored to achieve miniaturization are, meandering the lines to create a folded microstrip resonator [10], and the use of capacitively loaded transmission lines [1].

In the case of the folded microstrip resonator, size is reduced by meandering the lines to form a folded ring structure. This level of miniaturization is determined by the number of meandering sections and the tightness of the meanders. The level of compactness achievable is however limited by parasitic coupling which occurs if adjacent lines are located too close to each other.

In the case of the capacitively loaded microstrip loop resonator, miniaturization is achieved by using open stubs placed at regular intervals inside the loop. The stubs provide capacitive loading and creates a slow wave effect.

3.2 Novel Closed Loop Resonator

This thesis proposes a novel closed loop resonator structure that achieves both miniaturization and improved coupling by using slow wave structures in the form of capacitively loaded transmission lines. CTL is applied on the closed loop resonator by placing stubs at regular intervals around the circumference. Unlike the previously explored structures, the new resonator structure uses both inward and outward pointing open stubs as shown in Figure 10 - Figure 12.

By using double stubs instead of single stubs, the loaded capacitance C_p can be doubled without increasing the total size, thus further reducing the phase velocity, resonant frequency and size. The stubs are spaced such that a stub of equivalent width can be slotted into the space between two stubs. This enables a structure similar to an interdigital capacitor to be formed when an identical resonator is placed in close proximity. The effect is an increase in coupling between resonators which aids filter synthesis.

This section demonstrates the effectiveness of resonator miniaturization using the new structure and formulates a method of synthesizing miniaturized closed loop resonators of a particular frequency. For standardization, the resonators shown from this point onwards are designed on Rogers Substrate RO6010, ε_r=10.2, h=25 mils.

Figure 9 to Figure 13 features square closed loop and miniaturized closed loop resonators which will be used to demonstrate resonator miniaturization and the effect of varying CTL parameters. To determine resonator characteristics, the resonators are weakly coupled to ports using 50Ω feed lines that are separated from the resonators by a 10 mil gap. This keeps loading to a minimal.

A brief description of each of the featured resonators is as follows:

a. Resonator square closed loop shown in Figure 9 is used as a reference for comparison against the miniaturised structures of similar size. Resonators shown in Figure 10, Figure 11, Figure 12 are miniaturised closed loop resonators designed with the CTL structure. These designs are such that the total length and width is equivalent to Figure 9. This enables performance comparison with respect to a fixed size to be made.

b. Resonator double_stub shown in Figure 10, features a simple case of a closed loop resonator with CTL. This will be used as a reference for comparison of the effects of varying various CTL parameters namely stub width and stub separation.

c. Resonator dbl_w35 shown in Figure 11, features a variant of Figure 10 with stub width increased by 50% from 23 to 35 mils. The stub width is selected such that a gap of 10 mils between the stubs is achieved when two resonators are placed together. This structure is created to demonstrate the effects of increasing stub width on resonance frequency.

d. Resonator Figure 12, features a variant of Figure 10 with the number of stubs per side increased. The distances between the stubs are selected such that a gap of 10 mils between the stubs is achieved when two resonators are placed together. This structure is created to demonstrate the effects of increasing the number of stubs on resonance frequency.

e. Resonator Figure 13, features a square closed loop resonator with resonant frequency 1.08GHz, equal to that in Figure 12.

The frequency response plot of the resonators is shown in Figure 14. A bar chart to compare the resonance frequency is shown in Figure 15.

Substrate: Rogers 6010 h=25mils, $\varepsilon_r = 10.2$

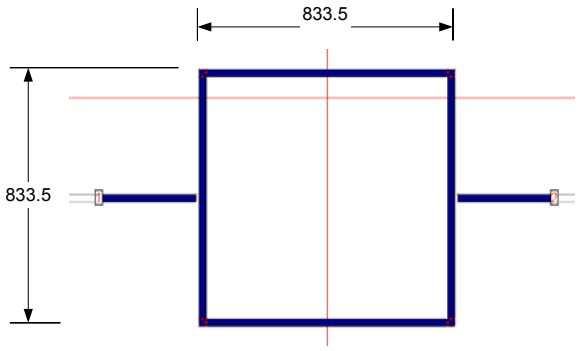

Figure 9: Square closed loop f_0=1.42 GHz

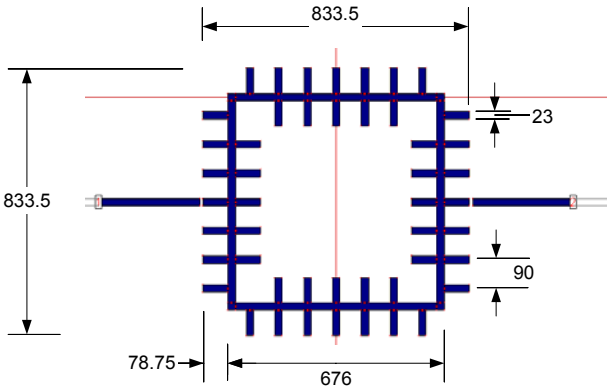

Figure 10: Double_stub f_0=1.19 GHz

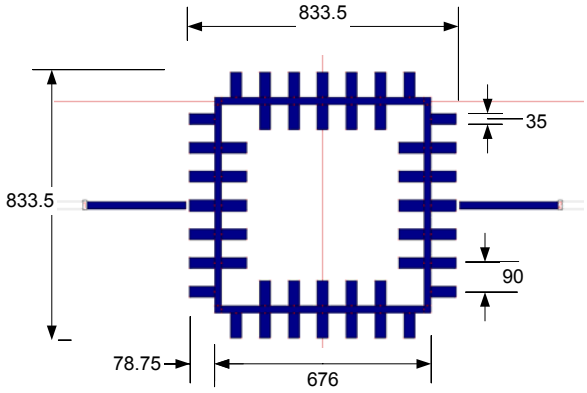

Figure 11: dbl_w35 f_0=1.14 GHz

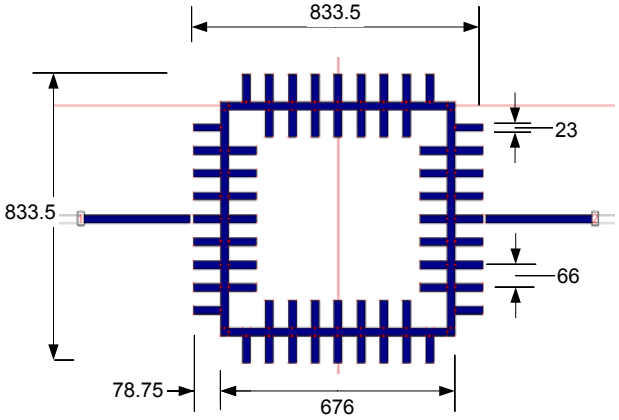

Figure 12: dbl_d66 f_0=1.08 GHz

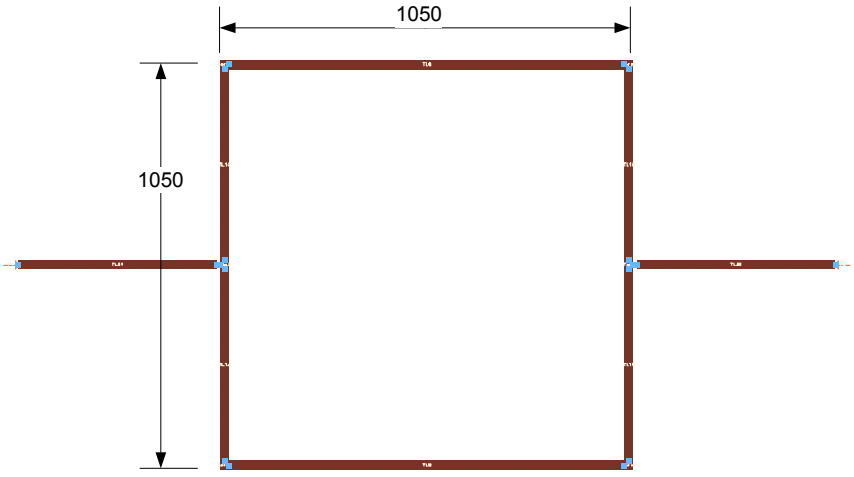

Figure 13: Square closed loop at f_0=1.08 GHz

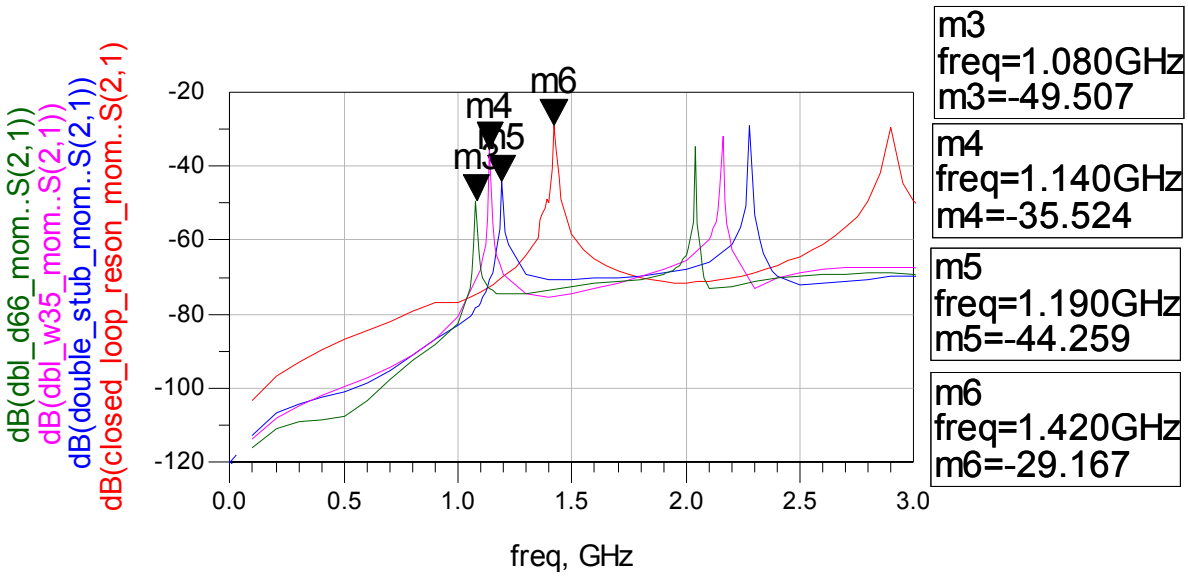

M3 dbl_d66 M5 double_stub

M4 dbl_w35 M6 square closed loop

Figure 14: Resonator frequency response

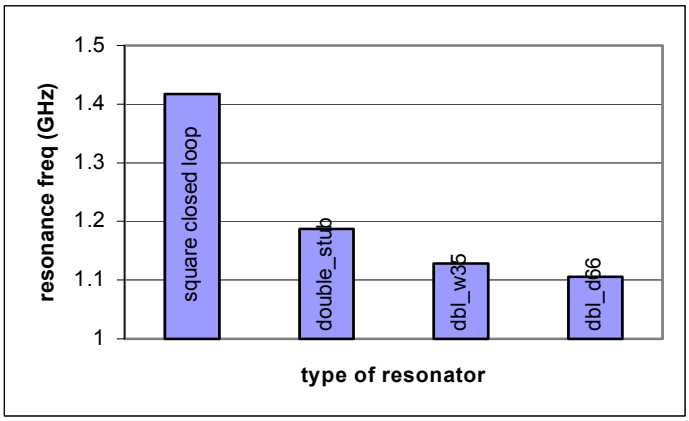

Figure 15: Compare resonance frequency

Resonator Miniaturization

To demonstrate resonator miniaturization, two resonators with equivalent resonant frequency are compared.

- Miniaturized resonator shown in Figure 12 is compared against the
- Square loop resonator shown in Figure 13.

Comparing their sizes, the miniaturized resonator achieves 20% reduction in both horizontal and vertical dimensions and a 37% reduction in area. This shows the ability of the new structure to achieve miniaturization.

Varying CTL parameters

To demonstrate the effect of varying CTL parameters for a fixed resonator size, three resonators shown in Figure 10 to Figure 12 which occupy the same total length and width, are simulated using IE3D and compared.

From the simulation results in Figure 15, the effect of varying CTL parameters is observed:

- Increasing stub width causes resonant frequency to decrease as can be seen by comparing the resonant frequency of resonator double_stub shown in Figure 10 with dbl_w35 shown in Figure 11.
- Increasing number of stubs reduces resonant frequency as can be seen by comparing the resonant frequency of resonator double_stub shown in Figure 10 with dbl_d66 shown in Figure 12.

The above observations correspond with the properties of CTL structures described in 2.5.

Hence the results show that the new miniaturized resonator structure enables lower resonant frequency and hence miniaturisation to be achieved. In addition, it shows that the level of miniaturization can be controlled by varying the unit cell parameters.

3.3 Resonator Synthesis Procedure

Given a desired resonator frequency f_0, the procedure to generate a miniaturized closed loop resonator is illustrated in the flow chart in Figure 20. A detailed description of the procedure is as follows:

1) Specify the following resonator parameters:
   - f_0 – resonant frequency
   - Z_{OCTL} –characteristic impedance of the CTL unit cells and unloaded microstrip lines used to form the loop.

   To prevent mismatch within the loop, all unit cells and unloaded microstrip lines should use the same characteristic impedance.

2) Specify the combination of unit cells used to form the sides of the resonator. This involves specifying the type, number and electrical length of the unit cells used to form each side of the resonator. For the case of a square resonator, each side has an electrical length of ϕ=90°. A suggested unit cell combination consists of:
   - N_{dbl_stub} double stub cells,
   - 2 single stub cells and
   - 2 unloaded transmission lines at the corner for tuning.

   This combination encourages the maximization of double stub cells in the design to enable further miniaturization. In the design, the single stub cells are placed at the sides due to obstructions near the corners and the unloaded microstrip lines are placed before the corners to aid fine tuning. As an example, the unit cell combination for the miniaturized resonator introduced earlier in Figure 12 consists of:
   - 7 double stub cells of electrical length 10° (N_{dbl_stub}=7, Φ_{dbl_CTL}=10°)
   - 2 single stub cells of electrical length 7° at the sides (N_{sgl_stub}=2, Φ_{sgl_CTL}=7°)
   - 2 unloaded TL at the corners of electrical length 3° (N_{TL}=2, Φ_{TL}=3°)

   A close up view of each side is shown in Figure 18. The electrical length of each side can be calculated using the formulae:

$$N_{TL}\phi_{TL} + N_{sgl\_stub}\phi_{Sgl\_CTL} + N_{dbl\_stub}\phi_{dbl\_CTL} \le 90^{\circ}$$

3) Calculate the dimensions of the single and double stub CTL unit cells.

The electrical length a CTL unit cell is given by the formulae:

$$\phi_{CTL} = \frac{d\omega_0}{u_p} = d\omega_0\sqrt{L\left(C + \frac{C_p}{d}\right)} \quad .$$

where ω_0 is the frequency of interest, L and C are related to the transmission line characteristic impedance and loading [4].

The procedure to design a microstrip CTL is as follows:

a) First set the characteristic impedance of the unloaded unit cell Z_0 and determine the required stub capacitance C_p as follows:

$$Z_0 = \sqrt{\frac{L}{C}} > \left(Z_{0CTL} = \sqrt{\frac{L}{C + \frac{C_p}{d}}} \right) \qquad (\Omega)$$

$$C_p = \frac{\phi_{CTL}\left(Z_0^2 - Z_{CTL}^2\right)}{\omega Z_0^2 Z_{CTL}} \qquad (\mathrm{F})\,.$$

Note that for the case of double stub unit cells, each stub can be assumed to provide a load capacitance of $C_p/2$.

b) With Z_0, the parameters of the unloaded microstrip line can be calculated:

W_{TL} - width of unloaded microstrip line

u_p - phase velocity of unloaded microstrip line

ε_e - effective dielectric constant

$$\varepsilon_e\left[w_{TL}\right] = \frac{\varepsilon_r + 1}{2} + \frac{\varepsilon_r - 1}{2}\frac{1}{\sqrt{1 + \left(12h / W_{TL}\right)}}$$

$$u_p = \frac{c_0}{\sqrt{\varepsilon_e\left[w_{TL}\right]}} \quad (\mathrm{ms}^{-1})$$

c) Specify the desired phase velocity of the loaded CTL unit cell u_{pCTL}, and calculate unit cell length d.

$$u_{pCTL} < u_p \qquad (\mathrm{ms}^{-1})$$

$$d = \frac{\Phi_{CTL} u_{pCTL}}{\omega} \qquad (\mathrm{m})$$

d) Select a suitable stub width W_{stub} such that coupling between adjacent stubs is minimized. A suggested distance between stubs is *d-2h,* where *h* is the substrate thickness. Calculate the stub dimensions shown in Figure 16 and Figure 17:

Z_{stub} characteristic impedance of stub

Φ_{stub} electrical length

l_{stub} physical length of stub

$$\phi_{stub} = \tan^{-1}\left[\omega C_p Z_{stub}\right] \quad \text{(rad)}$$

$$l_{stub} = \frac{\phi_{stub}}{\omega C_p} \quad \text{(m)} .$$

e) Simulate the unit cell using EM simulation. Tune the structure to the correct electrical length by adjusting l_{stub} until the desired electrical length is achieved. Store the final S-parameter file for resonator synthesis.

4) Cascade the cells to form the desired resonator. The resonator can be modelled and simulated using ADS by using the unit cell S-parameter data and microstrip transmission line models as shown in Figure 19.

5) Tune the resonator to the required frequency by adjusting the length of the unloaded transmission lines l_{TL} at the corners of the square resonator. This parameter is chosen because it is the most predictable and easiest to modify. The use of circuit simulation instead of EM simulation for tuning enables significant reduction in simulation time. The final design can be verified by performing an EM simulation and comparing with the circuit simulation results. The results are expected to be similar if coupling between stubs is kept minimal.

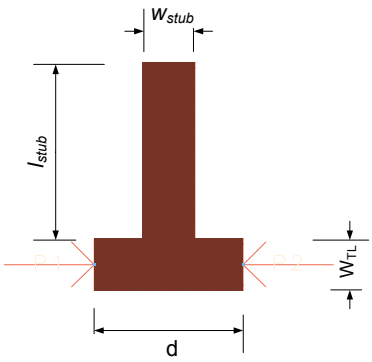

Φsgl_stub= electrical length of single stub cell

Figure 16: Single stub unit cell

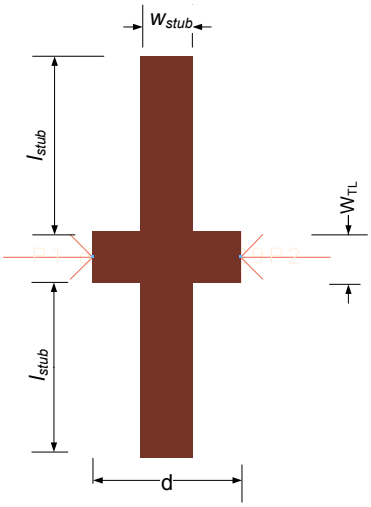

Φdbl_stub= electrical length of double stub cell

Figure 17: Double stub unit cell

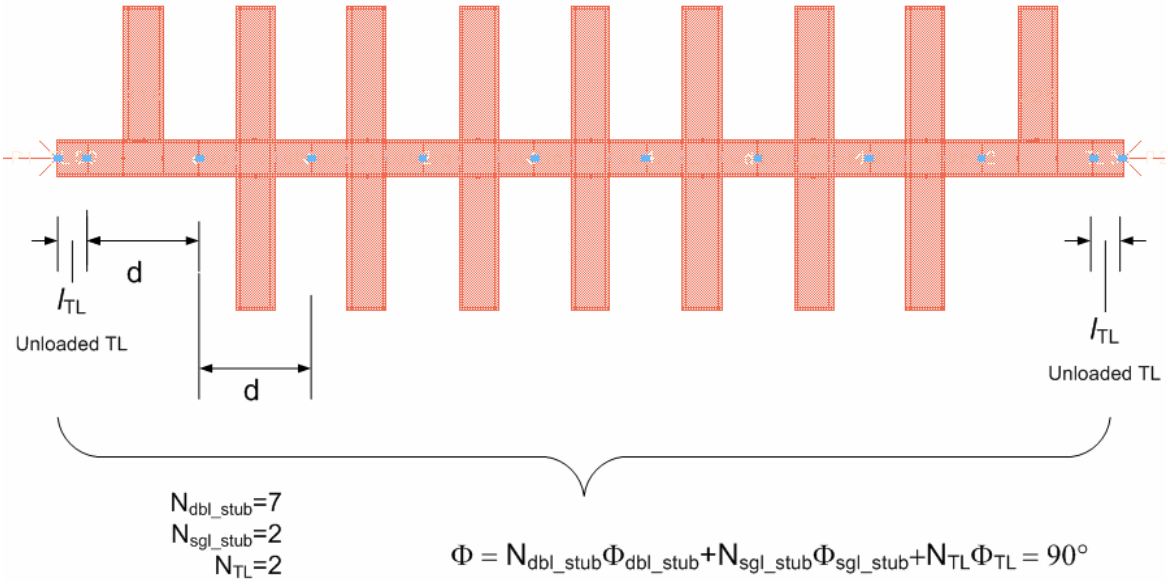

Figure 18: Cascaded unit cells for a single side

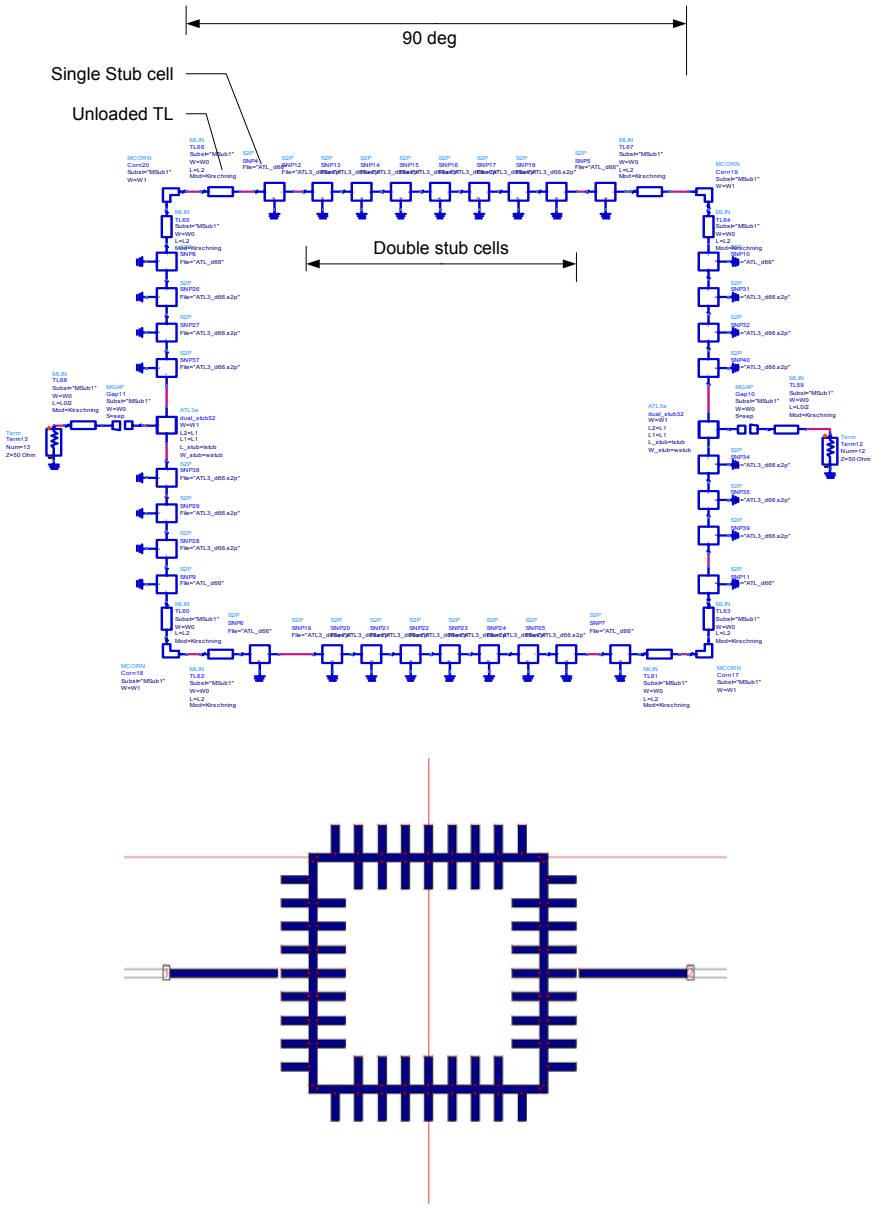

Figure 19: Circuit model of miniaturized resonator in ADS

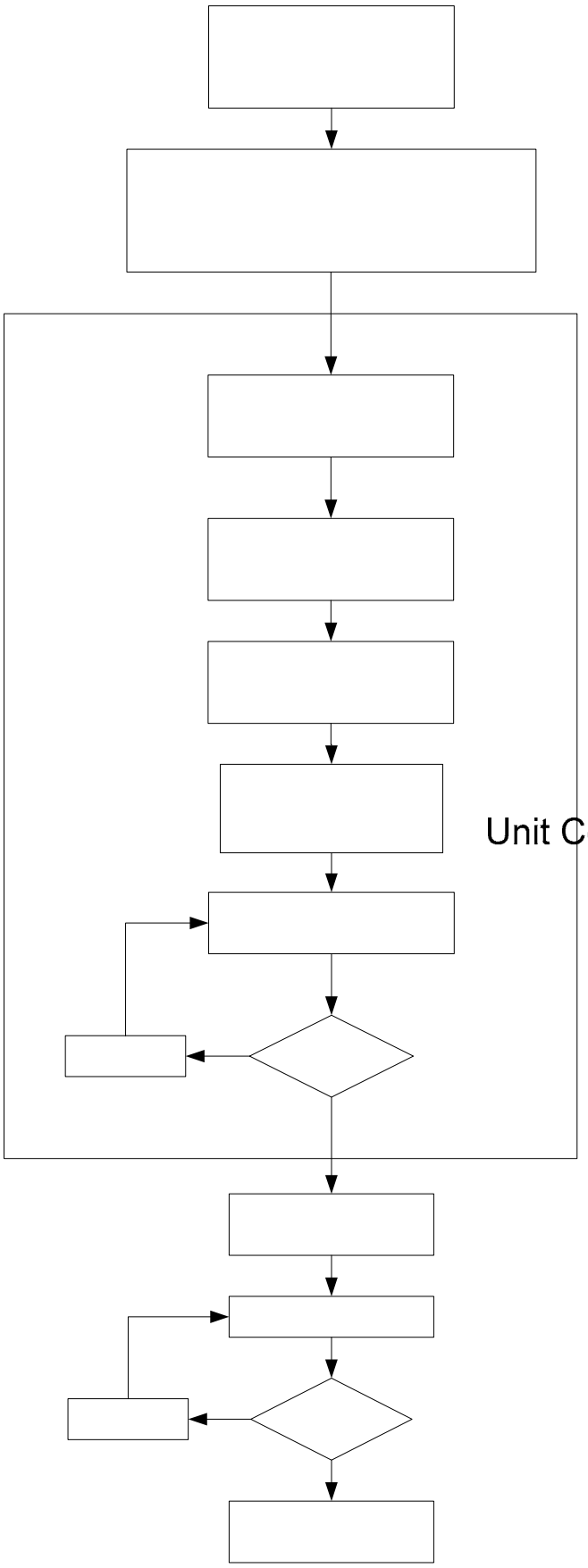

Figure 20: Resonator Synthesis Procedure

3.3.1 Example

To demonstrate miniaturized resonator synthesis using the method described, an example is shown. In this example, the resonator will be simulated using various methods to display the effects of unit cell model accuracy on the final simulated result.

Resonator specifications: f_0=1.10 GHz, Z_{OCTL}= 30 Ω;
Substrate: RO6010 ε_r= 10.2 , h =25 mils.

1) The unit cell combination is chosen to be as follows:
   - dual stub CTL - N_{dbl_stub} =7, ϕ_{dbl_CTL} = 10°
   - single stub CTL - N_{sgl_stub} =2 , ϕ_{sgl_CTL} = 7°
   - unloaded TL - N_{TL} =2, ϕ_{TL} = 3°

2) The unit cell synthesis procedure is applied to determine unit cell parameters.
   First, the characteristic impedance of unloaded unit cell is set: Z_0 = 50 Ω > Z_{0CTL} =30 Ω

   The required stub capacitance is calculated using $C_p = \dfrac{\phi_{CTL}\left(Z_0^2 - Z_{CTL}^2\right)}{\omega Z_0^2 Z_{CTL}}$ (F).

   For the double stub unit cell, the net capacitive loading provided by the two stubs is calculated to be C_p=0.68pF.
   Hence the capacitance provided by each stub can be assumed to be C_{p_stub}=0.34pF

   With Z_0=50 Ω the unloaded transmission line parameters are determined:

   $W_{TL} = 23$ (mils)
   $u_p = 1.147 \times 10^8$ (ms^{-1})

   The unit cell phase velocity is arbitrary selected as u_{p_CTL}=*0.56* u_p

   The unit cell length is calculated using $d = \dfrac{\Phi_{CTL} u_{pCTL}}{\omega} = 66$ (mils).

Setting W_{stub}=23 mils, the stub parameters are calculated

$$Z_{stub} = 50\ \Omega$$

$$l_{stub} = \frac{\phi_{stub}}{\omega C_{p\_stub}} = 1.93 \quad (\text{mm}) = 78.75 \quad (\text{mil}).$$

Double Stub CTL

To highlight the difference in simulation results, the double stub unit cell is simulated using both ADS circuit models shown in Figure 22 and EM simulation as shown in Figure 21. The simulated results are shown Figure 23. The results show that the EM simulation results (Marker m2) differs from the circuit simulation (Marker m1) by approximately 0.61°. This equates to approximately 6% error at the desired frequency. Hence the use of circuit models should be avoided in this example.

d = 66 mil

W_{TL} =23 mil

W_{stub}=23 mil

l_{stub}=78.75 mil

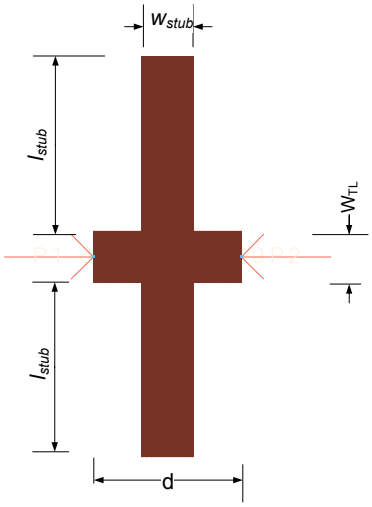

Figure 21: Double stub EM model

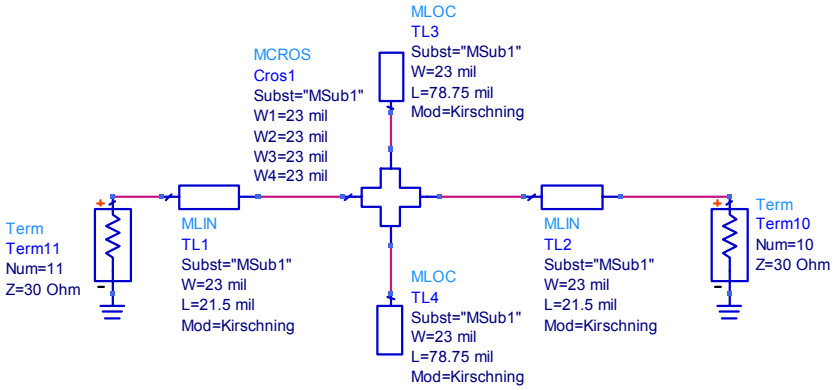

Figure 22: Double stub ADS circuit model

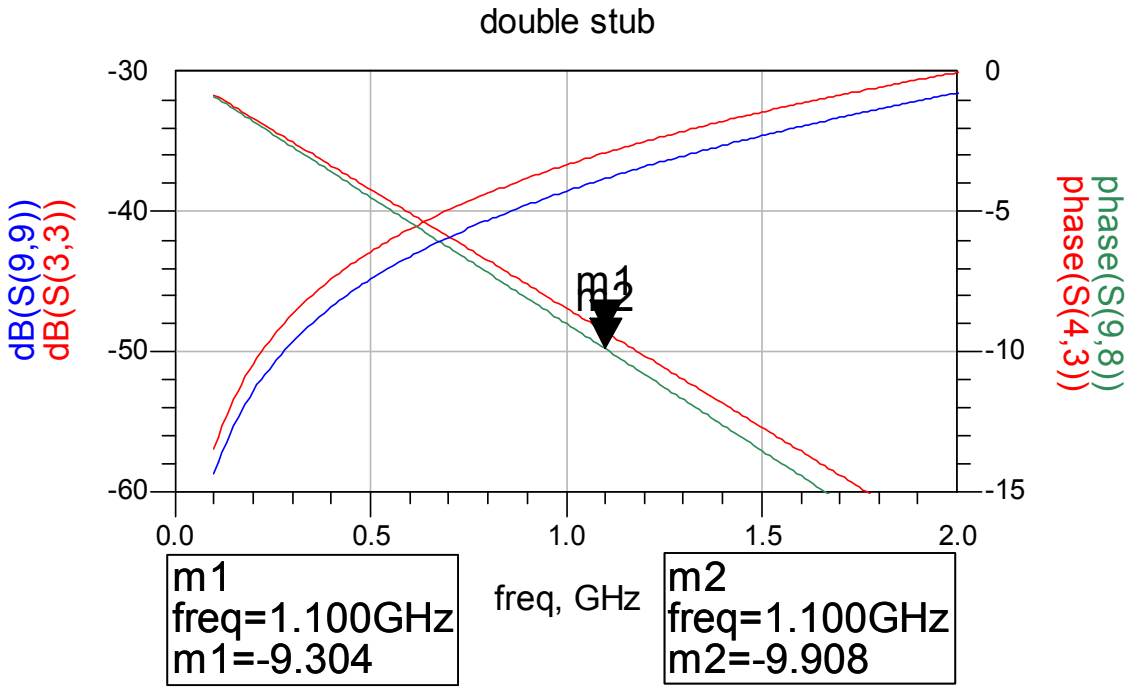

Figure 23: Double stub response

Single Stub CTL

To enable structure symmetry, the single stub unit cells are created to be of the similar dimension as the double stub unit cells. To highlight the difference in simulation results, the single stub unit cell is simulated using both ADS circuit models shown in Figure 25 and EM simulation as shown in Figure 24. The simulated results illustrated in Figure 26 shows that the EM simulation results (Marker m2) differs from the circuit simulation results (Marker m1) by approximately 0.8°. This equates to approximately 9% error at the desired frequency. Hence the use of circuit models for single stub unit cells should be avoided in this example.

d = 66 mil

W_{TL} =23 mil

W_{stub}=23 mil

l_{stub}=78.75 mil

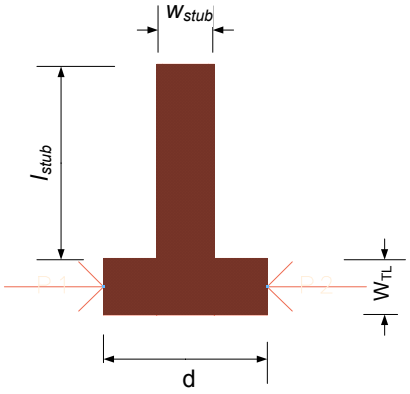

Figure 24: Single stub EM model

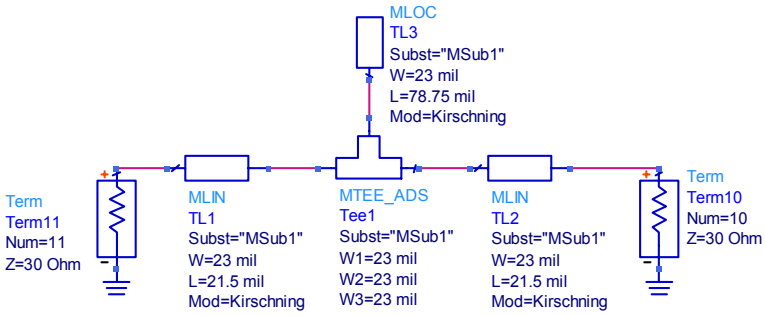

Figure 25: Single stub circuit model

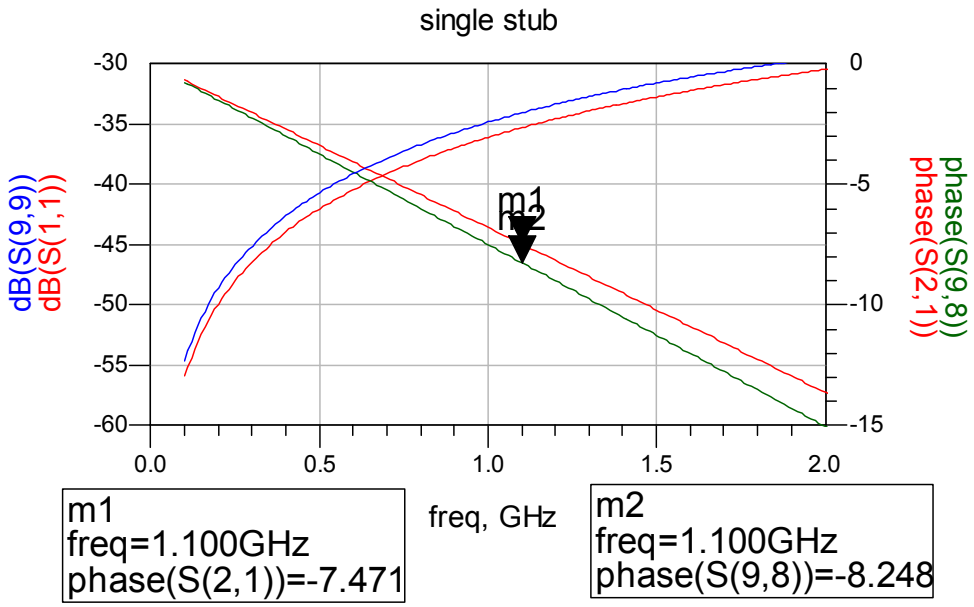

Figure 26: Single stub response

3) The miniaturized closed loop resonator is formed by cascading the synthesized unit cells as shown in Figure 27. To overcome inaccuracies in the circuit models for the unit cells, the S-parameter results from EM simulations are used to model the cells. The resonator is simulated using circuit simulation, and the unloaded microstrip lines at the corners are tuned to l_{TL} =18 mils.

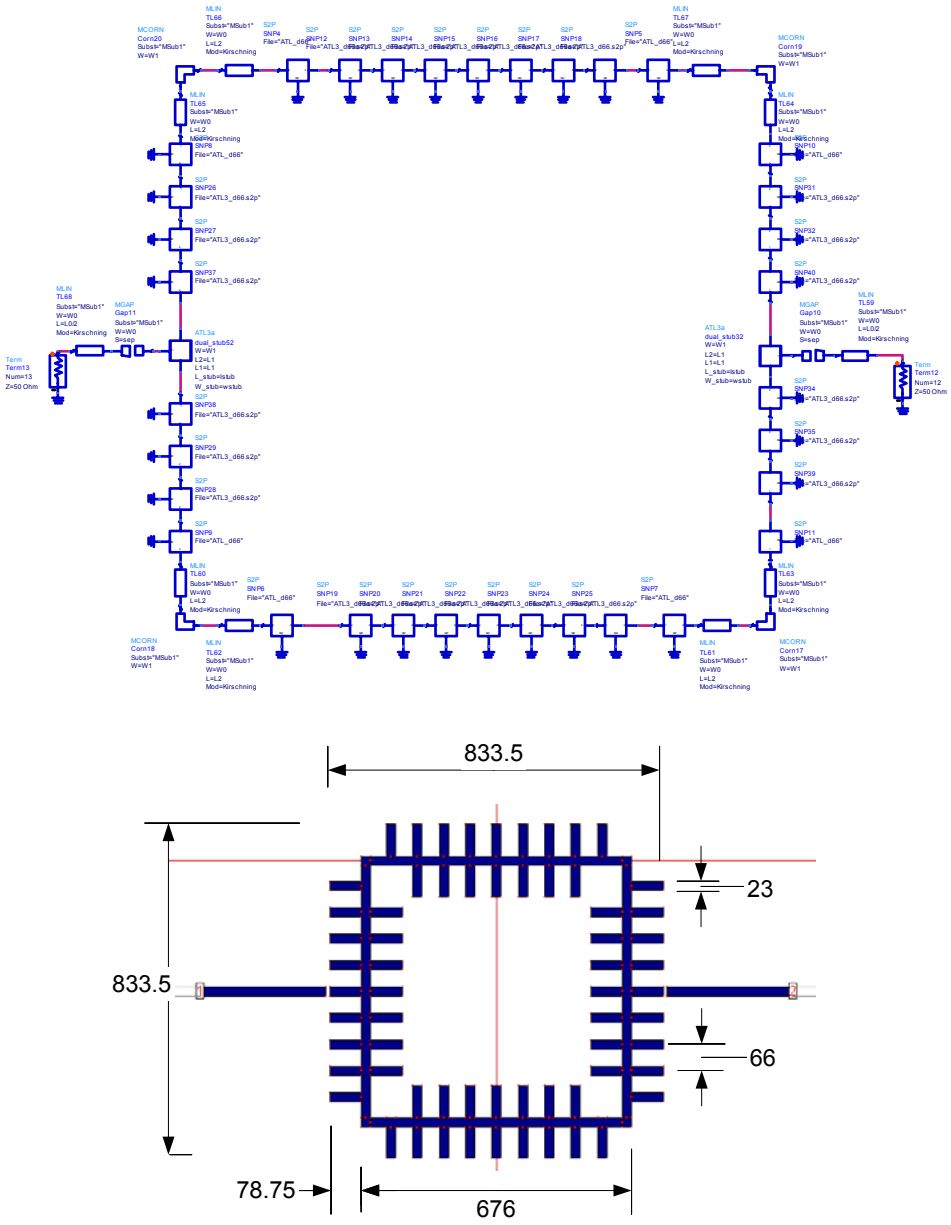

Figure 27: Synthesized resonator

4) To compare simulation accuracy, the resonator is modelled and simulated using three different methods namely circuit simulation, EM simulation and hybrid circuit simulation where S-parameter model of the unit cells are used. The simulated results are shown in Figure 28.

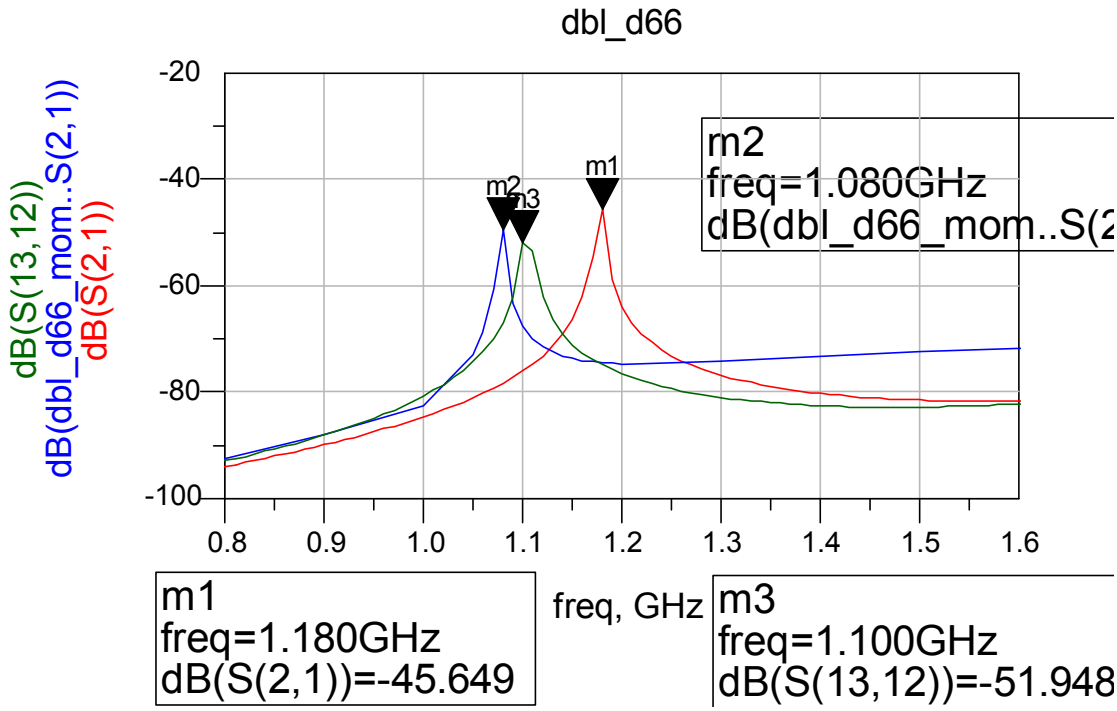

Figure 28: Synthesized resonator dB|S21|

Marker m1 displays the circuit simulation results where the unit cell is modelled using microstrip line and microstrip T-junction models in ADS.

Marker m2 displays the EM simulation results and is used as a reference.

Marker m3 displays the hybrid circuit simulation results where the unit cells are replaced with the S-parameters from EM simulation.

The results show that the circuit simulation (Marker m1) is inaccurate and differs significantly from the EM simulation results. This occurs due to inaccuracies in the circuit model of the unit cell which translates to error in the predicted electrical length. This error increases with the number of cascaded sections.

The hybrid circuit simulation (Marker m3) on the other hand provides a close approximation and differs from the EM simulation results by only 0.02 GHz which is less than 2% error.

Hence this shows that the design methodology provides a fairly effective method for designing the miniaturized resonators.

3.4 Summary

The example has provided a simple demonstration of how a miniaturized resonator of a desired frequency can be synthesized. To achieve further size reduction, the following parameters can be varied:

- Increase the number of stubs N_{dbl_stub}
- Reduce the distance between stubs d
- Increase stub width W_{stub}
- Increase stub length l_{stub}

However, these parameters cannot be increased indefinitely due to layout, coupling and fabrication constraints. Hence achieving maximum size reduction is a constraint optimization problem and will not be covered in this thesis.

Chapter 4 : Filter Synthesis Using Arbitrary Resonator Structures

4.1 Band Pass Filters

Bandpass filters may be defined by only three entities [7]; a resonator structure, coupling K between resonators (internal coupling) and coupling to the terminations Q_1 & Q_n (external coupling).

A straight forward design procedure based on these concepts begins with a prototype defined by k and q values. The values may be derived from the lowpass prototype g values as follows

Normalized:

$$q_1 = g_0 g_1$$

$$q_n = \begin{cases} g_n g_{n+1} & \text{n odd} \\ \dfrac{g_n}{g_{n+1}} & \text{n even} \end{cases} \qquad k_{i,i+1} = \frac{1}{\sqrt{g_i g_{i+1}}} \quad \text{for } i = 1 \text{ to } n-1.$$

The k and q values are normalized to a fractional bandwidth of one.

Denormalized:

$$Q_1 = q_1 \frac{f_0}{BW} \qquad K_{i,j} = k_{i,j} \frac{BW}{f_0}.$$

$$Q_n = q_n \frac{f_0}{BW}$$

The denormalized values are obtained by including a non-unity fractional bandwidth factor.

With the denormalized K and Q values, filter synthesis can be performed in two ways:

The values can be used with analytical expressions to design a bandpass filter by finding element values. This method is used to design top-C filters. [8]

Design of coupled resonator filters with any arbitrary resonator structure by using an empirical method.

In this project, arbitrary resonator structures are used, hence the second method will be elaborated in the subsequent sections.

4.2 Coupled Resonator Filter

There is a general technique for designing coupled resonator filters in the sense that it can be applied to any type of resonator regardless of physical structure. It has been applied to waveguide filters, ceramic filters and microstrip filters. This design method is based on coupling coefficient of intercoupled resonators and external Q-factors of the input and output resonators. [5]

4.2.1 General Coupling Matrix for Coupled Resonator Filters

This method is derived from the *General Coupling Matrix*, which is used to represent a wide range of coupled-resonator filter topologies. The matrix is formulated from either a set of loop equations or a set of node equations. This leads to a set of formulae for analysis and synthesis of coupled-resonator filter circuits in terms of coupling coefficient *K* and external Q-factors.

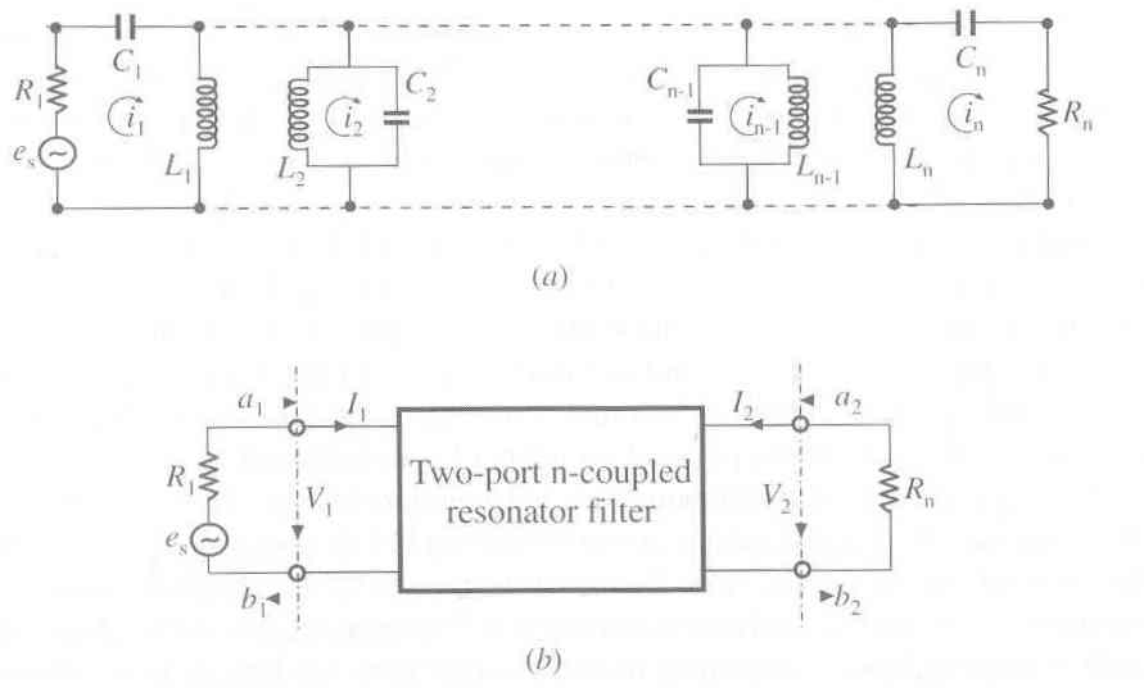

Figure 29: Equivalent circuit for n-coupled resonators (a) loop equation formulation, (b) network representation

Representation of the network in matrix form leads to:

$$\begin{pmatrix} R_1 + \frac{1}{j\omega C_1} + j\omega L_1 & j\omega L_{12} & \cdots & j\omega L_{1n} \\ -j\omega L_{21}\, i_1 & \frac{1}{j\omega C_2} + j\omega L_2 & \cdots & -j\omega L_{2n} \\ \vdots & \vdots & \vdots & \vdots \\ -j\omega L_{n1} & -j\omega L_{2n} & \cdots & R_n + \frac{1}{j\omega C_n} + j\omega L_n \end{pmatrix} \cdot \begin{pmatrix} i_1 \\ i_2 \\ \vdots \\ i_n \end{pmatrix} = \begin{pmatrix} e_s \\ 0 \\ \vdots \\ 0 \end{pmatrix}$$

$$[Z] \cdot [i] = [e]$$

For simplicity, consider a synchronously tuned filter where all resonators resonate at the same frequency $\omega_0 = \frac{1}{\sqrt{LC}}$, where $L = L_1 = L_2 = \ldots = L_n$ and $C = C_1 = C_2 = \ldots = C_n$. The impedance in matrix maybe expressed as

$$[Z] = \omega_0 \cdot L \cdot \mathrm{FBW} \cdot [\overline{Z}]$$

$$[\overline{Z}] = \begin{pmatrix} \frac{R_1}{\omega_0 L \cdot \mathrm{FBW}} + p & -j\,\frac{\omega L_{12}}{\omega_0 L \cdot \mathrm{FBW}} & \cdots & -j\,\frac{\omega L_{1n}}{\omega_0 L \cdot \mathrm{FBW}} \\ -j\,\frac{\omega L_{21}}{\omega_0 L \cdot \mathrm{FBW}} & p & \cdots & -j\,\frac{\omega L_{2n}}{\omega_0 L \cdot \mathrm{FBW}} \\ \vdots & \vdots & \vdots & \vdots \\ -j\,\frac{\omega L_{n1}}{\omega_0 L \cdot \mathrm{FBW}} & -j\,\frac{\omega L_{n1}}{\omega_0 L \cdot \mathrm{FBW}} & \cdots & \frac{R_n}{\omega_0 L \cdot \mathrm{FBW}} + p \end{pmatrix}$$

Where the complex lowpass frequency variable:

$$p = j\,\frac{1}{\mathrm{FBW}}\left(\frac{\omega}{\omega_0} - \frac{\omega_0}{\omega}\right)$$

Note that:

$$\frac{R_i}{\omega_0 L} = \frac{1}{Q_{ei}} \text{ for } i = 1 \text{ to } n$$

Q_{e1} and Q_{en} are external Q-factors of the input and output resonators.

Define coupling coefficient

$$M_{ij} = \frac{L_{ij}}{L}$$

And assuming for narrowband approximation

$$\frac{\omega}{\omega_0} \simeq 1$$

The [Z] matrix can be simplified to:

$$[\bar{Z}] = \begin{pmatrix} \frac{1}{q_{e1}} + p & -jm_{12} & \cdots & -jm_{1n} \\ -jm_{21} & p & \cdots & -jm_{2n} \\ \vdots & \vdots & \vdots & \vdots \\ -jm_{n1} & -jm_{n2} & \cdots & \frac{1}{q_{en}} + p \end{pmatrix}$$

where

Normalized external Q factors:

$$q_{ei} = Q_{ei} \cdot \mathrm{FBW} \quad \text{for } i = 1 \text{ to } n$$

Normalized Coupling coefficient:

$$m_{ij} = \frac{M_{ij}}{\mathrm{FBW}}$$

By inspecting the circuit and the network, it can be identified that $I_1 = i_1$, $I_2 = -i_n$, and $V_1 = e_s - i_1 R_1$. Since

$$a_1 = \frac{e_s}{2\sqrt{R_1}} \qquad b_1 = \frac{e_s - 2 i_1 R_1}{2\sqrt{R_1}}$$

$$a_2 = 0 \qquad b_2 = i_n \sqrt{R_n}$$

we have

$$S_{21} = \frac{b_2}{a_1}\Big|_{a_2=0} = \frac{2\sqrt{R_1 R_n i_n}}{e_s}$$

$$S_{11} = \frac{b_1}{a_1}\Big|_{a_2=0} = 1 - \frac{2 R_1 i_1}{e_s}$$

Solving for i_1 and i_n , we obtained

$$i_1 = \frac{e_s}{\omega_0 L \cdot \mathrm{FBW}} \cdot [\bar{Z}]_{11}^{-1} \qquad i_n = \frac{e_s}{\omega_0 L \cdot \mathrm{FBW}} \cdot [\bar{Z}]_{n1}^{-1}$$

Substituting the above, we have

$$S_{21} = \frac{2}{\sqrt{q_{e1} \cdot q_{en}}} \cdot [\bar{Z}]_{n1}^{-1}$$

$$S_{11} = 1 - \frac{2 R_1}{q_{e1}} \cdot [\bar{Z}]_{n1}^{-1}$$

4.2.2 General formulation for Extracting Coupling Coefficient K

The equations above may be incorporated into a general one:

$$S_{21} = \frac{2}{\sqrt{q_{e1} \cdot q_{en}}} \cdot [A]^{-1}_{n1}$$

$$S_{11} = \pm\left(1 - \frac{2R_1}{q_{e1}} \cdot [A]^{-1}_{n1}\right)$$

with [A]=[q]+p[U]-j[m]

where [q] is an n × n matrix with all entries zero, except for $q_{11} = \frac{1}{q_{e1}}$ and $q_{nn} = \frac{1}{q_{en}}$

[m] is the so called general coupling matrix, which is an n × n reciprocal matrix (i.e. $m_{ij} = m_{ji}$) and is allowed to have nonzero diagonal entries m_{ii} for an asynchronously tuned filter.

For a given filtering characteristic of S21 and S11, the coupling matrix and the external quality factors maybe obtained using synthesis procedures. Elements of the matrix [m] that emerge in general will have non-zero values. For asynchronously tuned filters, non-zero values only occur on the diagonal elements. If non-zero values lie everywhere else, means coupling exist between every resonator, this makes it impractical to be synthesized.

After determining the required coupling matrix for the desired filter characteristics, next step is to establish the relationship between the value of every required coupling coefficient and the physical structure of coupled resonators so as to find the physical dimensions of the filter for fabrication. Couplings can be positive or negative. Positive coupling enhances the stored energy of uncoupled resonators.

The universal formulation for extracting coupling coefficient is given by:

$$k = \pm \frac{1}{2}\left(\frac{\omega_{02}}{\omega_{01}} + \frac{\omega_{01}}{\omega_{02}}\right)\sqrt{\left(\frac{\omega_2^2 - \omega_1^2}{\omega_2^2 + \omega_1^2}\right)^2 - \left(\frac{\omega_{02}^2 - \omega_{01}^2}{\omega_{02}^2 + \omega_{01}^2}\right)^2}$$

For synchronously tuned resonators, it simplifies to

$$k = \pm \frac{f_2^2 - f_1^2}{f_2^2 + f_1^2}$$

To determine the coupling K between two resonators, the resonators are weakly coupled to the ports and S21 is measured. The coupling coefficient is determined from the resonant peaks of |S21| using the above formulae.

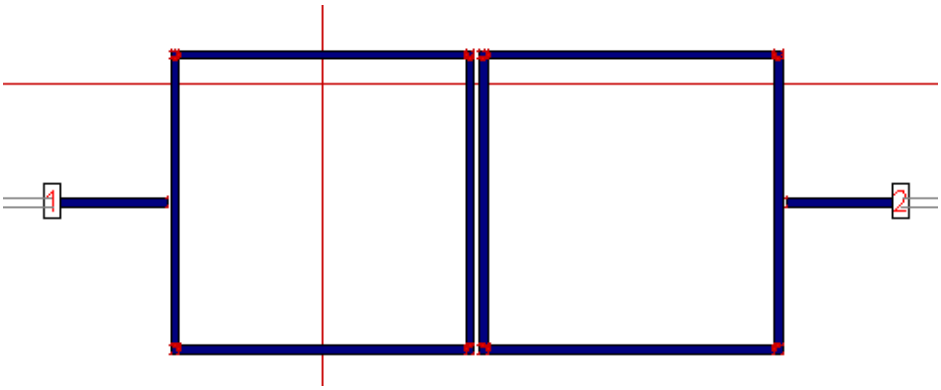

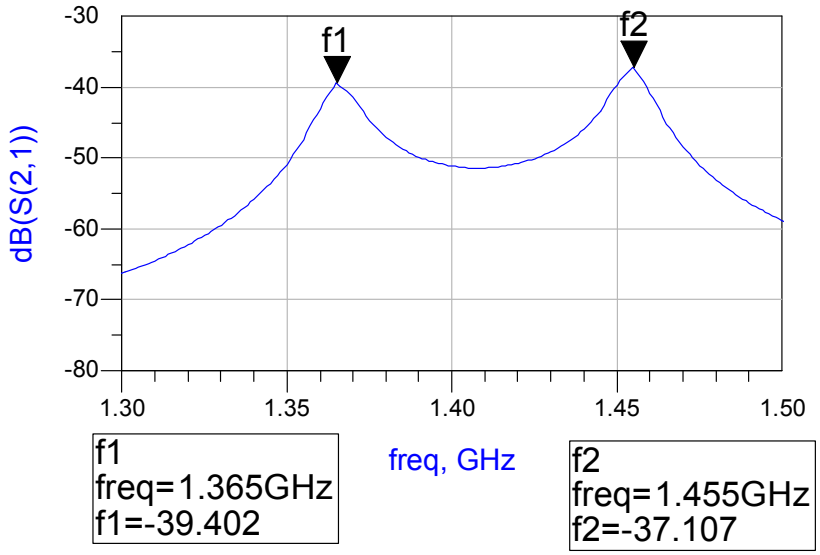

4.2.3 Formulation for Extracting External Quality Factor Q_e

Two typical input output structures for coupled microstrip resonator filters are the tapped line and the coupled line structure.

For tapped line coupling, usually a 50ohm feed line is directly tapped onto the resonator and the coupling or Q-factor is controlled by the tapping position. The closer the tapped line is to the virtual ground of the resonator, the weaker the coupling or larger the External Q-factor.

For coupled line coupling, the feed line is linked to a coupling structure, which is separated from the resonator by a gap. By reducing the coupling gap, a higher coupling and hence a lower external Q can be achieved.

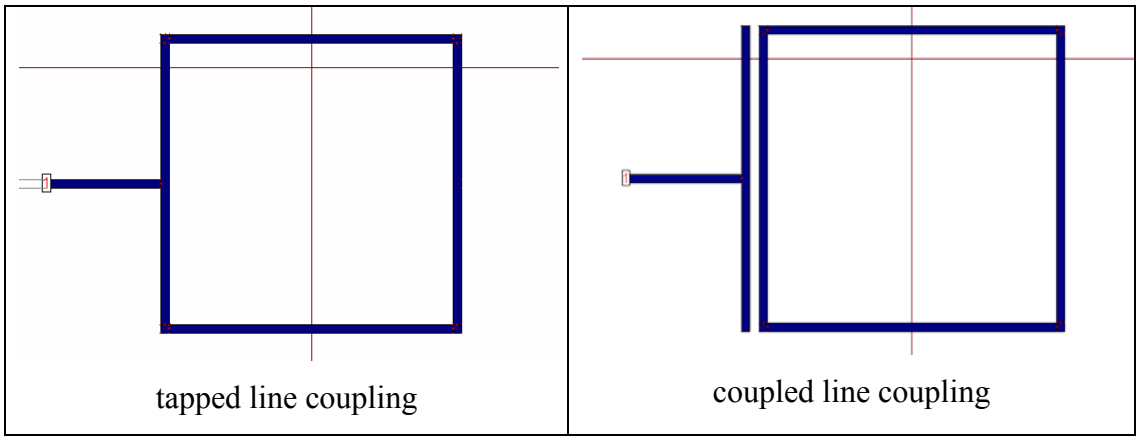

tapped line coupling

coupled line coupling

For a singly loaded resonator, the external Q-factor can be extracted from the phase of S11 using: $Q_s = \dfrac{\omega_0}{\Delta\omega_{\pm 90^\circ}}$

Shown in Figure 30 is the | S11| and phase S11 of a singly loaded resonator. The markers indicate ω_{+90}, ω_0 and ω_{-90}. These values are substituted into the above equation to determine singly loaded Q.

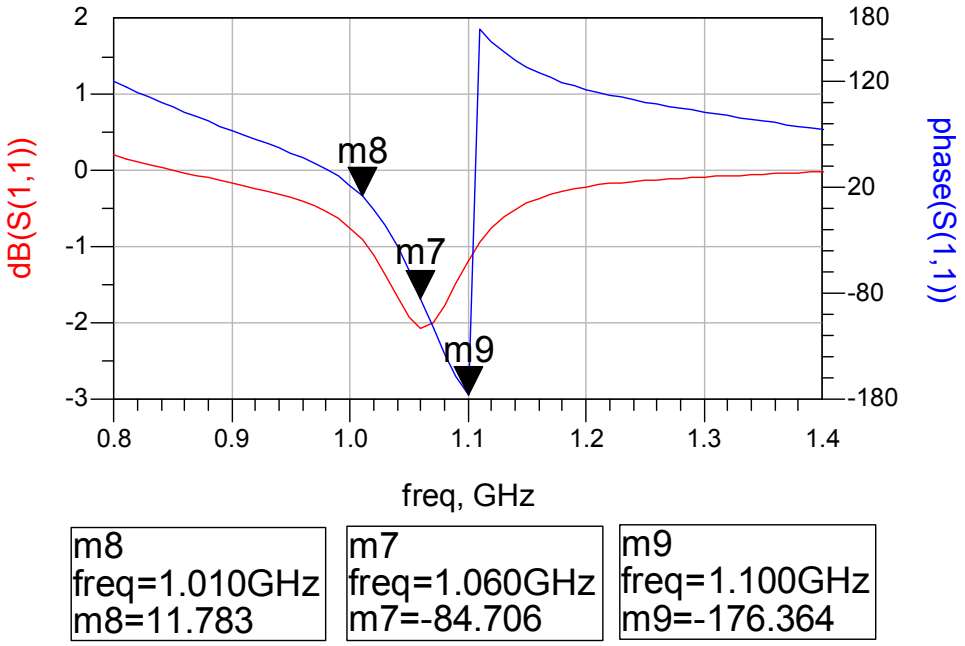

Figure 30: Singly loaded resonator S11

If the resonator is symmetrical, one could add another symmetrical load or port to form a 2-port network, hence creating a doubly loaded resonator. The external Q-factor of a doubly loaded resonator Q_d is extracted from the magnitude of S21. From there the external Q-factor singly loaded resonator Q_s can be determined below.

$$Q_s = 2Q_d = 2\frac{\omega_0}{\Delta\omega_{3dB}}$$

4.3 Procedure for Coupled Resonator Filter Design

The procedure for designing coupled resonator filters with arbitrary resonator structures is briefly summarized below:

1. Compute desired filter passband Q given by $Q_{bp} = \frac{f_0}{BW}$
2. Based on the type and order of filter, determine the lowpass prototype g values and from there calculate coefficients *q* & *k* and de-normalize the coefficients to obtain:

$$Q_1 = Q_{bp} \times q_1 \qquad K_{i,j} = \frac{k_{i,j}}{Q_{bp}}$$
$$Q_n = Q_{bp} \times q_n$$

3. From the plot of *K* vs. spacing between resonators, determine the required spacing between each resonator.
4. From the plot of Q_S vs tap location, determine the port tap or coupling position.

Note:

The *k* and *q* values tabulated are based on infinite inductor Q_U. In practice satisfactory results are obtainable for $Q_U \geq 10\ Q_{bp}$. This method assumes that coupling between non-adjacent resonators is not present.

Chapter 5 : Loaded Q and Coupling Coefficient of Resonators

5.1 Introduction

To perform coupled resonator filter synthesis, the range of achievable values for loaded Q_L and coupling coefficient K of a resonator must first be determined.

The miniaturized resonator dbl_d66 synthesized in the example on section 3.3.1 is chosen for filter synthesis (see Figure 27). This chapter begins by exploring methods for controlling external Q_L. Next the range of achievable Q_L and K values for the synthesized resonator are determined.

5.2 Loaded Q of Resonators

To determine the range of achievable Q_L, various different feed structures to the resonator have been simulated. The feed structures are generally divided into two categories:

1. Coupled line coupling (for high loaded Q) ;
2. Tapped line coupling (for low loaded Q) .

5.2.1 Coupled Line Coupling

For this method, the resonator is coupled by a feed line structure separated from the resonator by a gap g. Here two different feed structures are explored:

a) Parallel coupled line (Figure 31)
b) Coupled line with interdigital stubs (Figure 32)

The parallel coupled line feed consists of a straight line located parallel to the resonator. This feed structure is commonly used and examples of which can be found in the following references. [1], [10].

The coupled line with interdigital stubs feed merges with the resonator dbl_d66 to create a structure similar to an interdigital capacitor. This improves coupling and hence increases the port loading of the structure.

For both feed structures, external Q_L can be controlled by varying the gap distance between the feed structure and the resonator. The singly loaded Q is determined from |S21| using the formulae: $Q_s = 2Q'_d = 2\dfrac{\omega_0}{\Delta\omega_{3dB}}$.

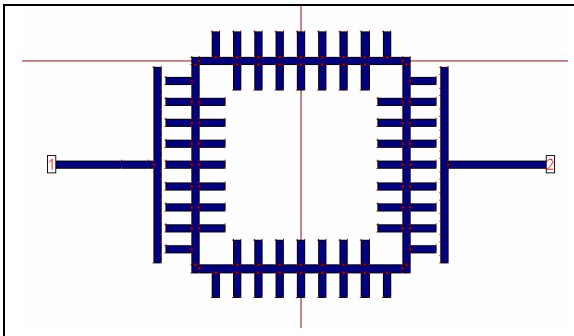

Figure 31: Parallel coupled line feed

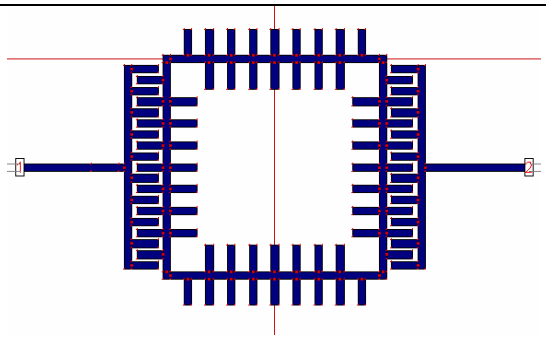

Figure 32: Coupled line with interdigital stubs feed

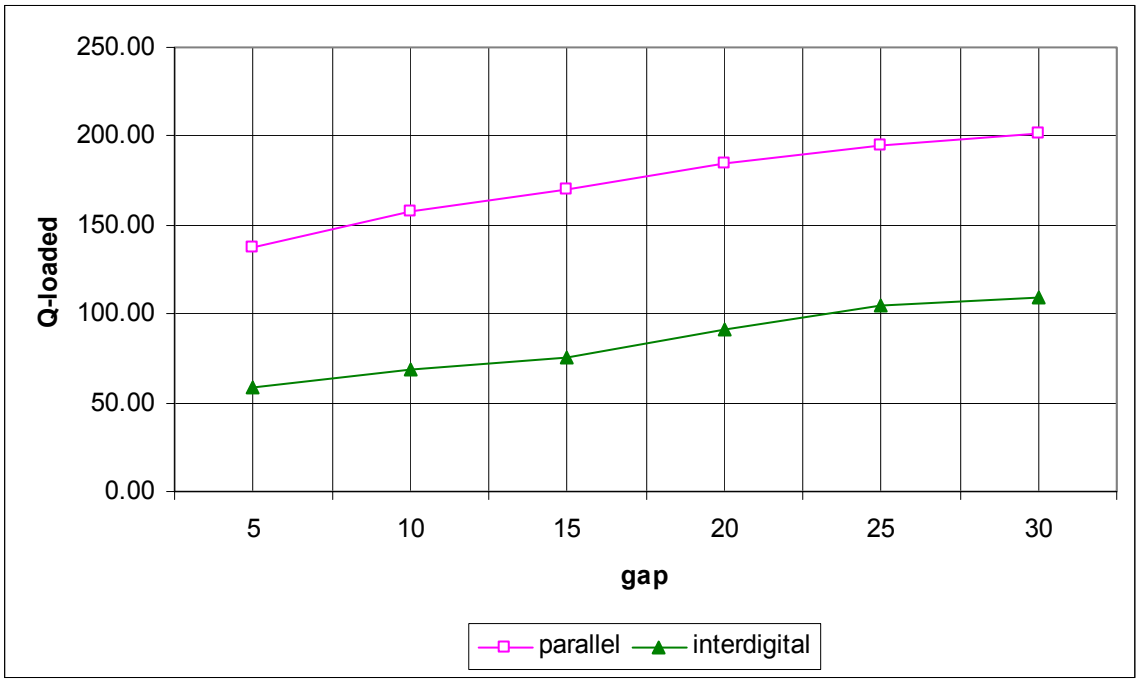

Figure 33: Coupled line Q_L

The loaded Q of the structures for different gaps are simulated and compared. The results in Figure 33, show that the Coupled line with interdigital stubs feed structure achieves a significantly lower Q_L compared to the Parallel coupled line feed structure. This proves that the interdigital structure provides a stronger coupling compared to the parallel coupled line structure and is hence preferred due to the wider range of Q_L values achievable.

Alternate Methods to Control Coupling of Interdigital Feed

Aside from varying the gap, the loaded Q provided by the interdigital feed can also be controlled by:

a) Varying the number of stubs. This alters the capacitive coupling from feed to resonator and changes Q_L. Shown in Figure 34 are interdigital feed structures with varying number of stubs but with the gap fixed at 15 mils. The results in Figure 35 show that increasing the number of stubs reduces Q_L due to the increased coupling provided by the feed structure.

b) Varying the stub length of the feed to alter the capacitive coupling. This option is currently unexplored in this thesis.

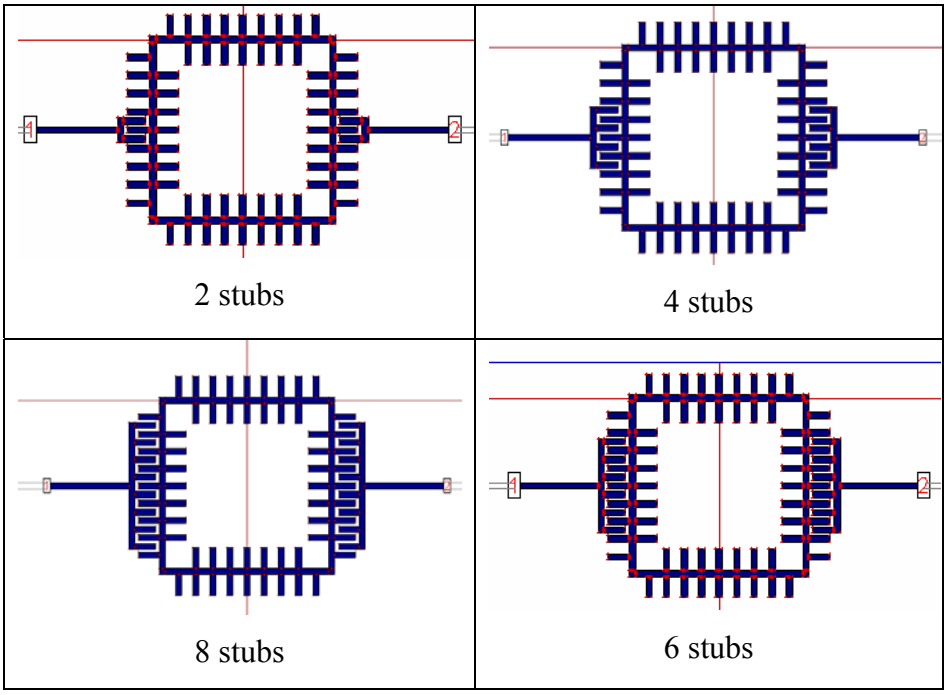

Figure 34: Coupled line with X interdigital stubs (gap=15 mils)

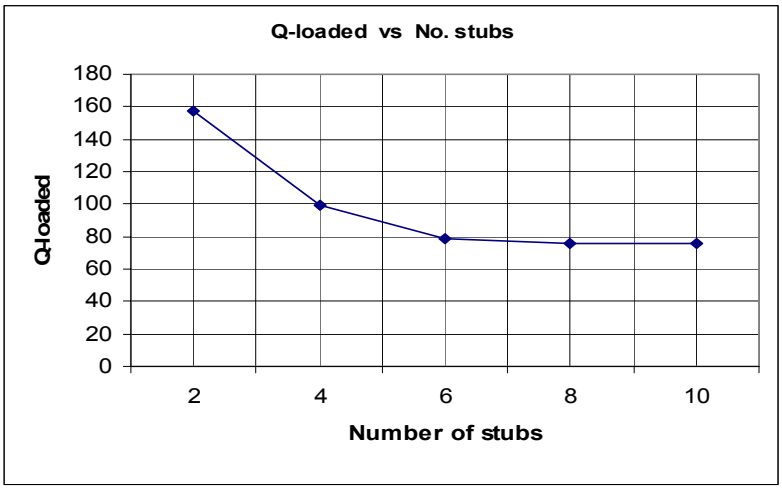

Figure 35: Q_L vs no. of stubs

5.2.2 Tapped Line Coupling

Tapped line coupling is used when low values of Q_L are required. The feed line usually in the form of a 50 ohm line is directly linked to the resonator structure. Q_L can be varied using two different methods:

1. Placing lumped inductors in series with the feed as shown in Figure 38.
2. Using multiple tap feed structures. This method is used to achieve precise control of Q_L, and is to be applied in cases where fine control of lumped inductor L is unavailable.

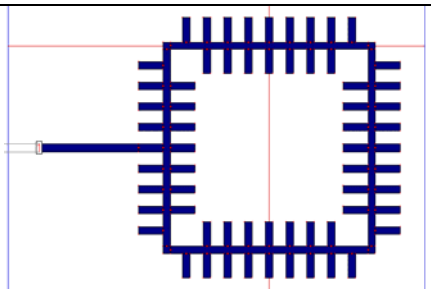

Figure 36: Tapped line coupling for dbl_d66

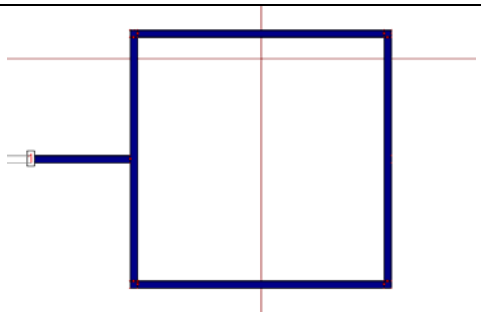

Figure 37: Tapped line coupling for Square closed loop resonator

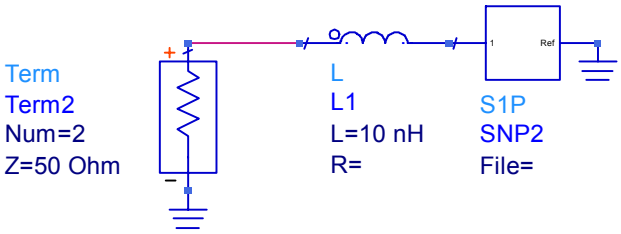

Figure 38: Tapped line with series inductor

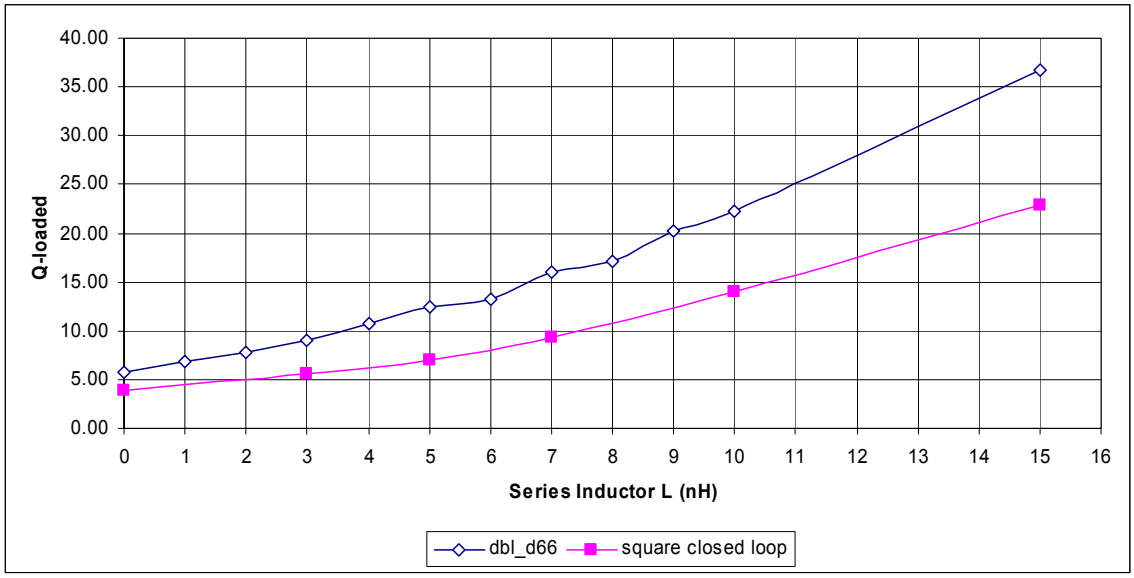

Figure 39: Effect of series inductor on Q_L

With the use of lumped inductors in the feed, each increment to the series inductance causes Q_L to be incremented accordingly as shown in Figure 39. The use of lumped inductors provides a convenient way of adjusting Q_L values as it to be changed easily. However in practice accurate control of lumped inductor values for L < 10 nH is difficult. This is significant when accurate control of Q_L is required.

To achieve precise control over Q_L, the multiple tap feed structures shown in Figure 40 are used. By varying the number of fingers or tap points, Q_L can be controlled to vary gradually over a small range ($5.89 < Q_L < 7.78$) Table 1. This is useful in applications where fine control of Q_L is needed. The multiple tap feed structure can also be used together with lumped inductors to achieve fine tuning at a higher range of Q_L.

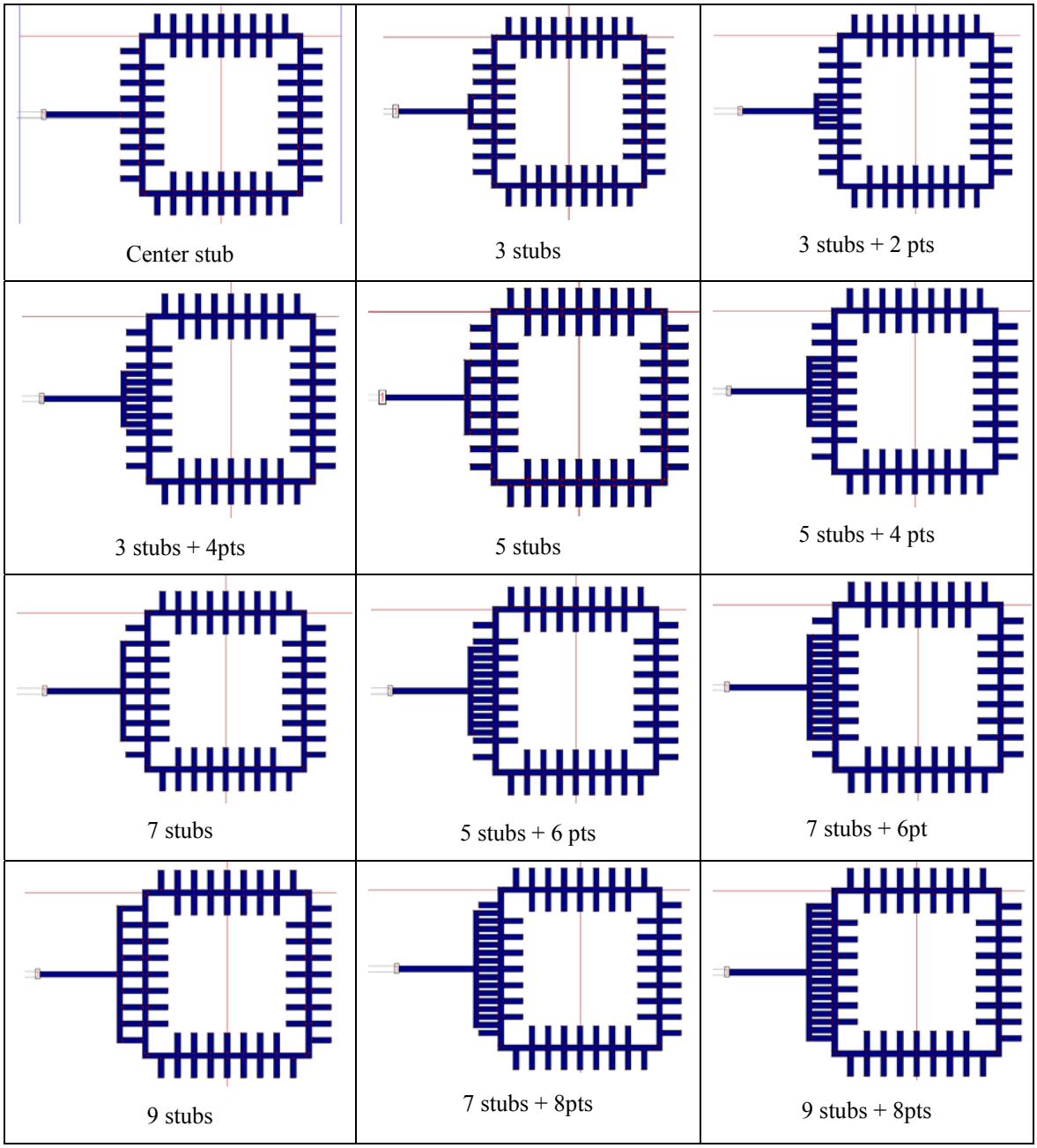

Figure 40: Multiple tap feed structures

Note: Detailed measurement results are shown in the reference.

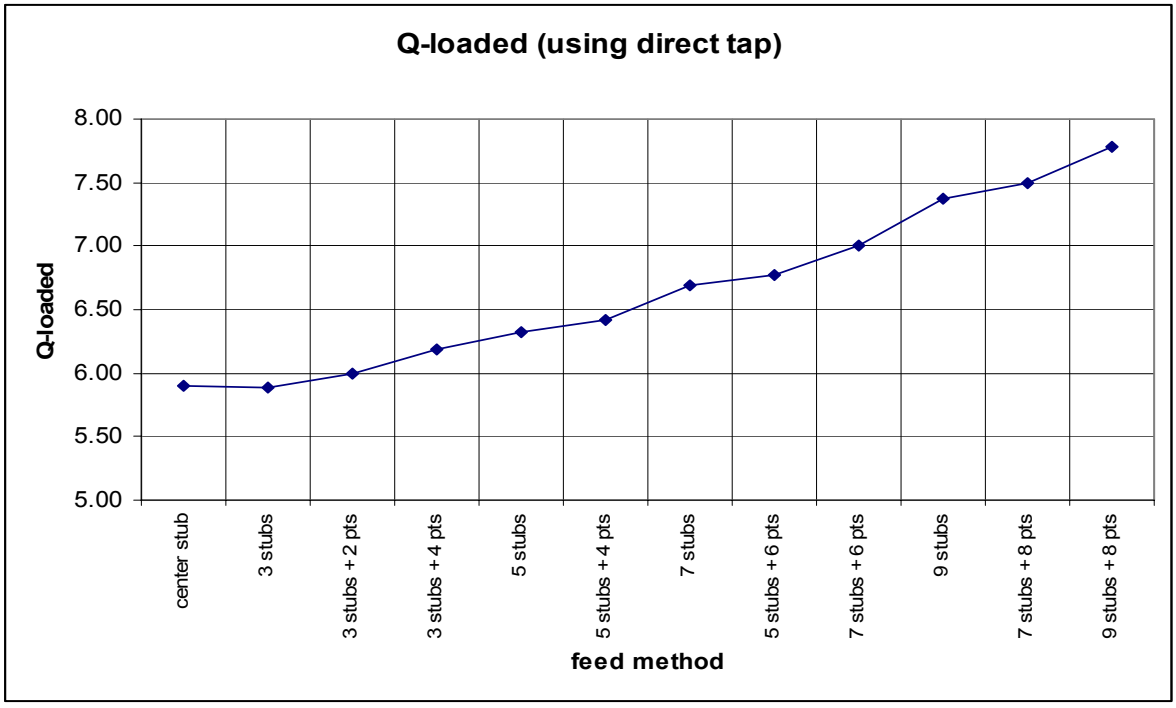

Figure 41: Q_L of tapped line coupled structures

Feeding structure	Q-loaded	ΔQ-loaded
Center stub	5.89	-
3 stubs	5.89	-
3 stubs + 2 pts	6.00	0.11
3 stubs + 4 pts	6.19	0.3
5 stubs	6.32	0.43
5 stubs + 4 pts	6.42	0.53
7 stubs	6.69	0.8
5 stubs + 6 pts	6.77	0.88
7 stubs + 6 pts	7.00	1.11
9 stubs	7.38	1.49
7 stubs + 8 pts	7.50	1.61
9 stubs + 8 pts	7.78	1.89

Table 1: Q_L of tapped line coupled structures for dbl_d66

5.2.3 Other Explored Feed Structures

This subsection introduces other feed structures and methods that have been explored in the process of development.

Varying feed location for Single Tap structure

Here, the effect of varying the tap location for a single tap structure on Q_L is explored. The "center stub" structure in Figure 40 represents the structure with zero offset. The structures with the shifted tap locations are shown in Figure 42.

The results displayed in Figure 43, shows that varying the tap location have little effect on Q_L. Moreover the variation with tap offset position is non-linear, hence this method is deemed to be non-effective for control of Q_L.

The minimal variation in Q_L with respect to tap position is due to the absence of forced boundary condition such as gaps. Hence despite the shift, the ring is still analyzed as two half wavelength resonators connected in parallel.

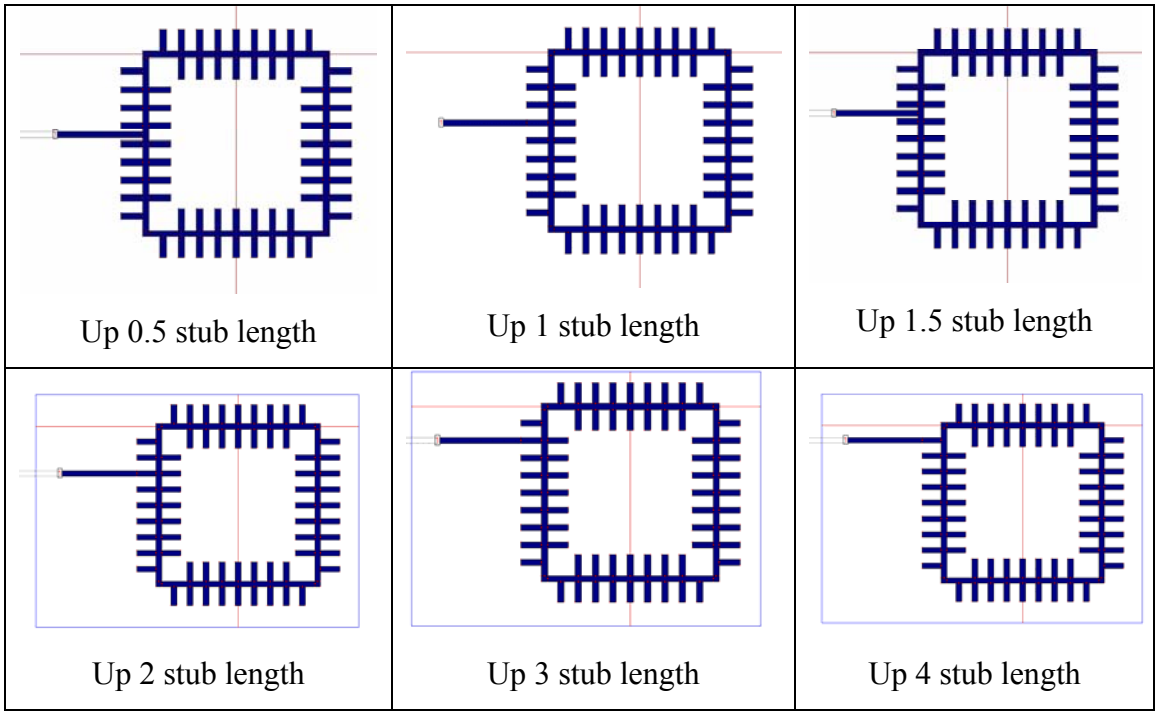

Figure 42: Single tap with vertical shifted tap positions

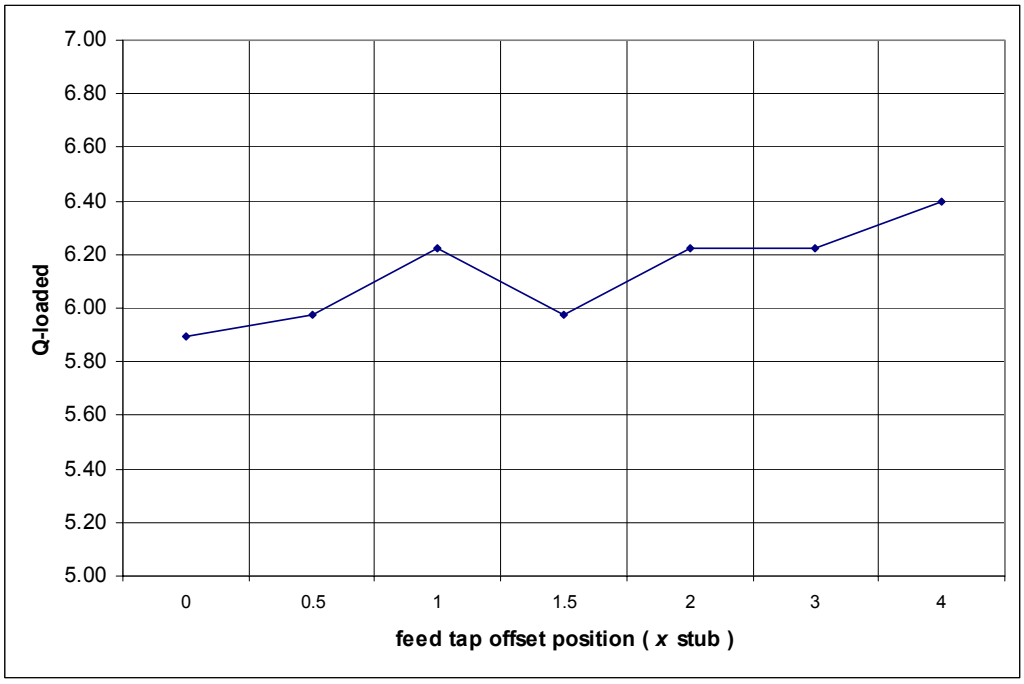

Figure 43: Single tap Q-loaded vs Offset

Varying feed location for Multiple Tap structure

The effect of shifting the feed location for the multiple tapped resonator '9 stub + 8pts' shown in Figure 44 is explored here. For each of the figures, the tap location is shifted up by X stub length from the centre line. The results in Figure 45 shows Q_L varies in large steps and non-linearly with respect to offset. This is makes its shifted response unpredictable and hence impractical to be used as a method for Q_L control.

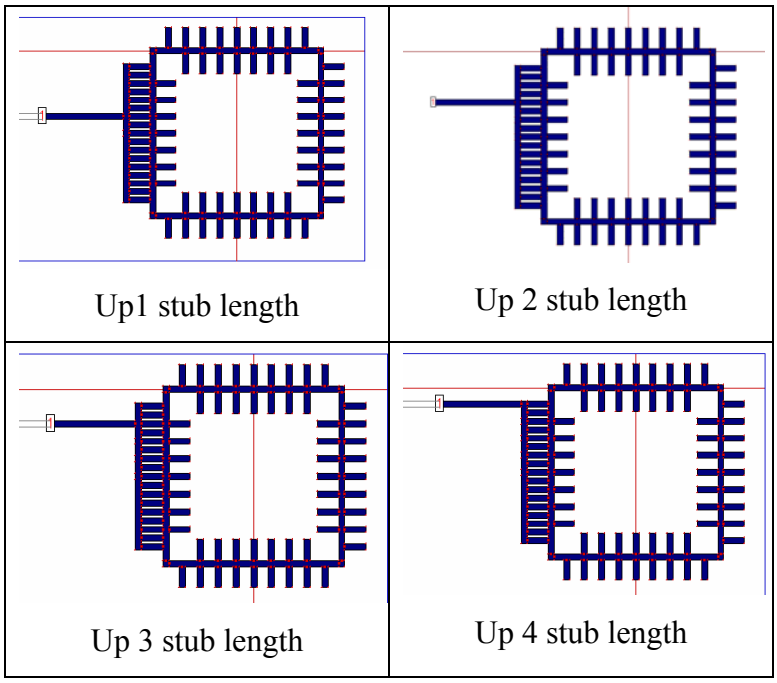

Figure 44: Multiple tap with vertical shifted feed positions

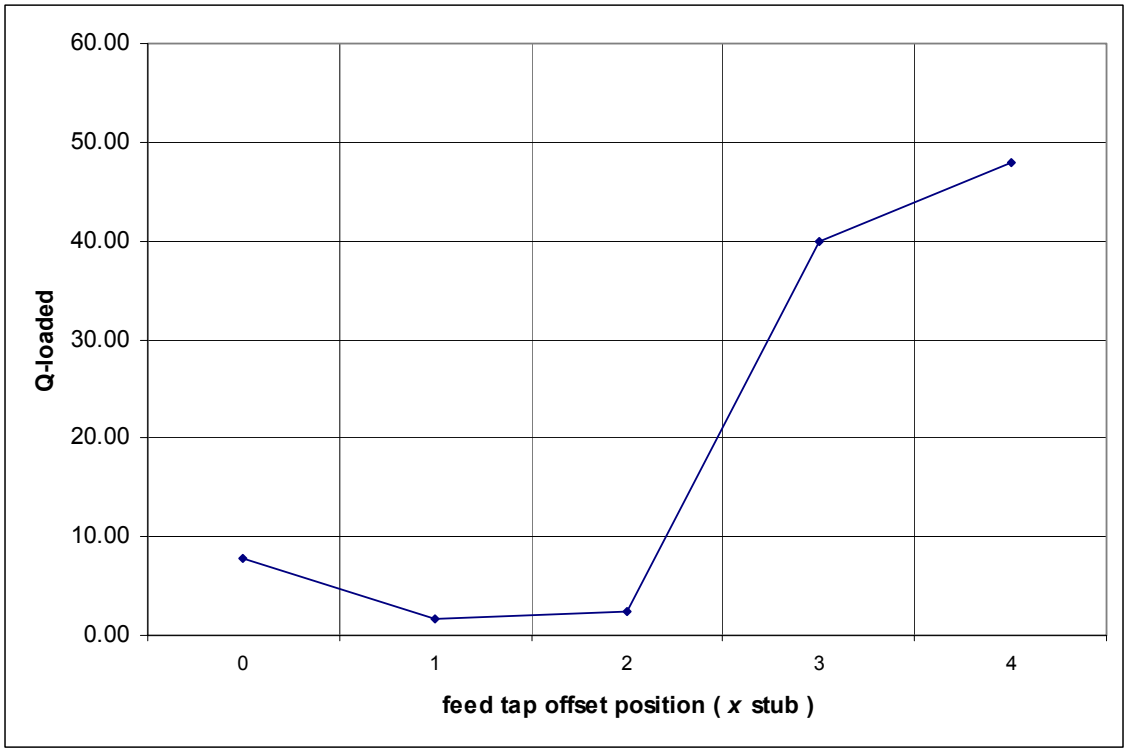

Figure 45: Multiple tap Q-loaded vs Offset

5.3 Coupling Coefficient K of Resonators

To determine the coupling K between closed loop resonator structures, the resonators are placed apart at varying gap distances and weakly coupled to the ports.

The coupling coefficient is determined from |S21| using the formula:

$$K = \frac{f_2^2 - f_1^2}{f_2^2 + f_1^2}$$

For resonator dbl_d66, strong coupling between the resonators is achieved by placing the structures such that the stubs resemble an interdigital capacitor Figure 46. The results are compared with that of the simple closed loop resonator where coupling occurs in the form of parallel coupled lines Figure 47.

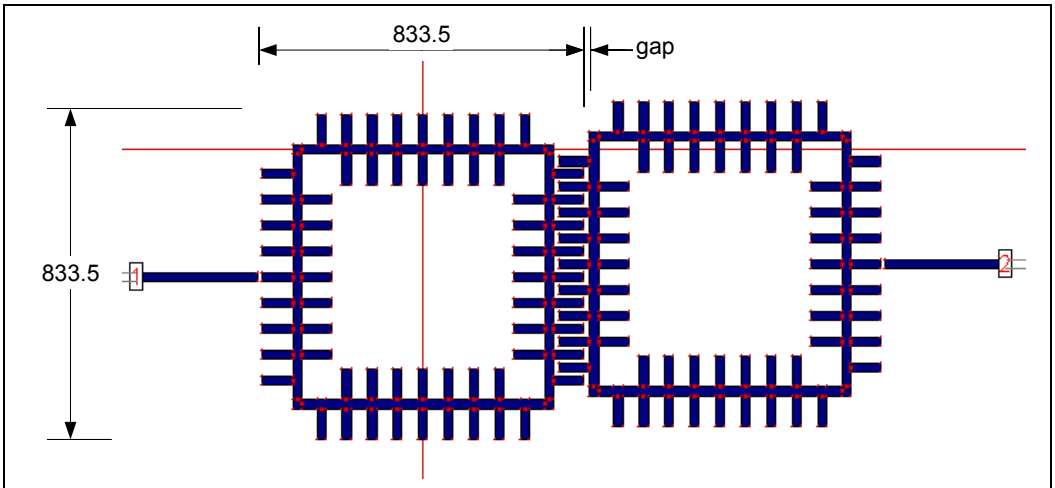

Figure 46: Coupling measurement of resonator dbl_d66

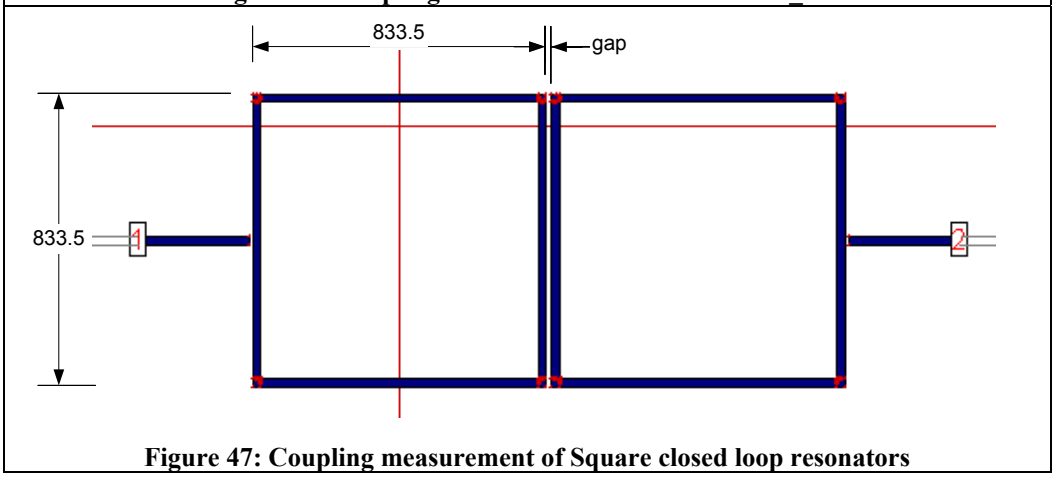

Figure 47: Coupling measurement of Square closed loop resonators

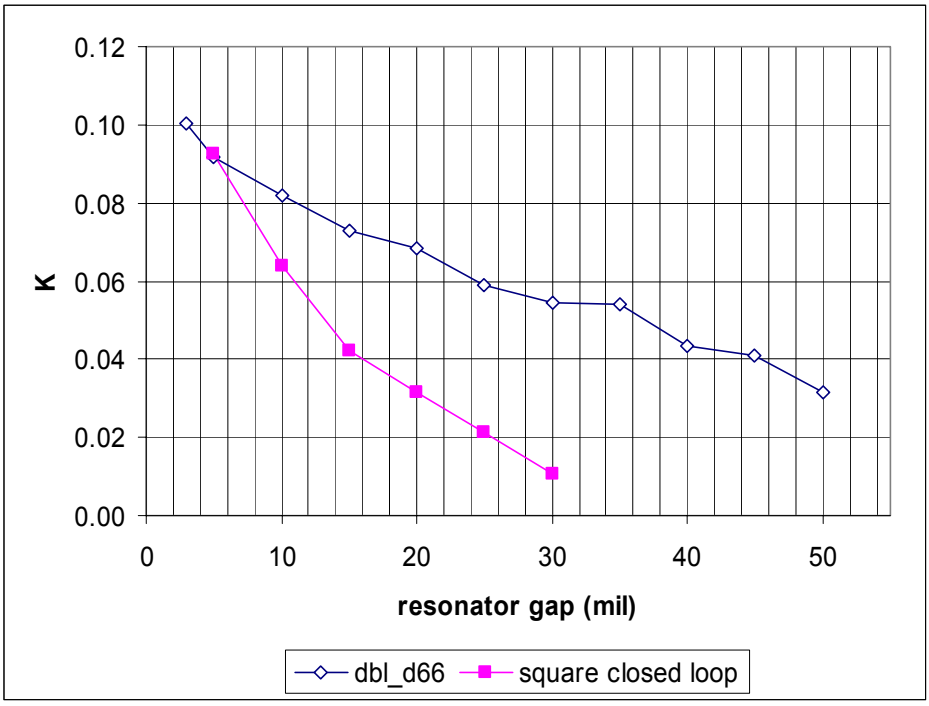

Figure 48: Coupling Coefficient K vs Gap

	K	
gap (mil)	Square Closed loop	Dbl_d66
5	0.09	0.09
10	0.06	0.08
15	0.042	0.073
20	0.032	0.068
25	0.021	0.059
30	0.011	0.055
35	Too weak	0.054
40	Too weak	0.044
45	Too weak	0.041
50	Too weak	0.032

Table 2: Coupling coefficient measurement results

Comparing the results, it is observed that:

1 For a gap > 5 mils, the coupling *K* achieved with resonator structure dbl_d66 in Figure 46 is larger than that of the closed loop resonator structure Figure 47.

2 Variation of *K* with gap is more gradual for resonator dbl_d66 hence sensitivity to fabrication tolerance is reduced. This enables more accurate control of *K*.

3 When two dbl_d66 resonators are coupled, a horizontal size reduction of one stub length 78.75 mils is achieved due to the interdigital structure.

5.4 Summary

In this chapter, feed structures for the miniaturized resonator have been explored and developed:

a) The interdigital feed structure extends the range of coupled line feed structures and is useful in situations where high Q_L values are required;
b) The multiple tap feed structure provides fine control at low loaded Q_L values.

The coupling coefficient of the miniaturized resonator has also been measured. The results show that new structure offers the following additional advantages over a Square closed loop resonator of equivalent size:

- Improved control of coupling coefficient K
- Size reduction when resonators are coupled.

The range of achievable Q_L and K values for resonator dbl_d66 have been characterized and the results are as follows:

Assuming a fabrication tolerance of gap $\geq$ 5 mils:

- Coupling coefficient: $K \leq 0.09$
- Q_L for tapped line coupling: $5.89 \leq Q_L \leq 7.78$
- Q_L for coupled line coupling: $Q_L \geq 58.9$

With these results, filter synthesis can be performed.

Chapter 6 : Miniaturized Closed Loop Resonator Filter

6.1 Introduction

In this section filter synthesis using the miniaturized closed loop resonator dbl_d66 will be demonstrated. The synthesized filter will be compared with one that is synthesized using the Square Closed Loop Resonator of equivalent size. Both filters are chosen to be Chebyshev with 0.01dB ripple and 10% bandwidth.

The K & external Q values for a Chebyshev filter of 0.01dB ripple with 10% bandwidth are shown in Table 3.

Coupling Coefficient K										Q-loaded	
N	**K12**	**K23**	**K34**	**K45**	**K56**	**K67**	**K78**	**K89**		**Qin**	**Qout**
1										0.96	0.96
2	0.2337									4.489	3.7046
3	0.128	0.128								6.292	6.292
4	0.1081	0.0794	0.1081							7.129	5.883
5	0.1007	0.0697	0.0697	0.1005						7.563	7.593
6	0.097	0.066	0.0621	0.066	0.097					7.814	6.448
7	0.0949	0.0641	0.0592	0.0592	0.0641	0.0949				7.97	7.97
8	0.0936	0.063	0.0577	0.0566	0.0577	0.063	0.0936			8.073	6.6624
9	0.0928	0.0607	0.0554	0.0554	0.0554	0.057	0.0624	0.0928		8.145	8.145

Table 3: Normalized K and Q values for Chebyshev filter 0.01dB ripple 10% bandwidth

6.2 Chebyshev Filter of 0.01dB Ripple, N=3, BW=10% Using Square Closed Loop resonator

The resonator square closed loop is determined in the previous chapter to have the following electrical characteristics:

Resonance Frequency: 1.42 GHz

Assuming a fabrication tolerance of gap $\geq$ 5 mils:

Coupling coefficient: $K \leq 0.09$

Q_L for tapped line coupling: $3.89 \leq Q_L \leq 22$

.

The *K* and *Q* values for a third order filter N=3 are approximately translated to the following physical parameters based on the previously simulated results in Figure 39 and Figure 48.

Coupling Coefficient K									Q-loaded	
N	**K12**	**K23**							**Qin**	**Qout**
3	0.128	0.128							6.292	6.292
Gap (mil)	5	5						**Feed structure**	Direct tap with 4nH inductor	

The synthesized filter structure is shown in Figure 49. Note that the lumped inductor is not shown. The structure occupies an area of 2.096 in^2 without the lumped inductors.

The structure is first simulated using EM simulation, next the S-parameter results are inserted into ADS circuit simulation as shown in Figure 50 to enable the effects of lumped inductors to be added. The final result plot in Figure 51 shows that the simulated results are reasonably close to that desired with the bandwidth deviating by approximately 3%.

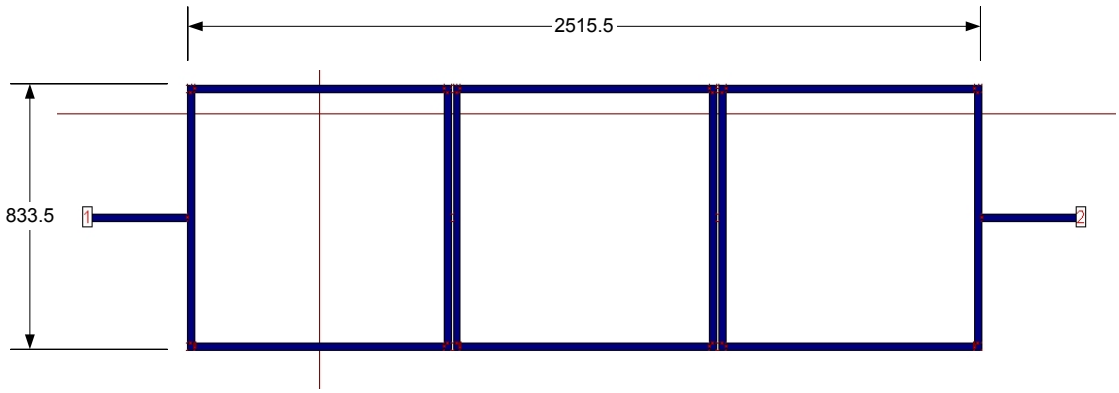

Figure 49: Layout of the 3rd order Chebyshev filter using Square closed loop resonator

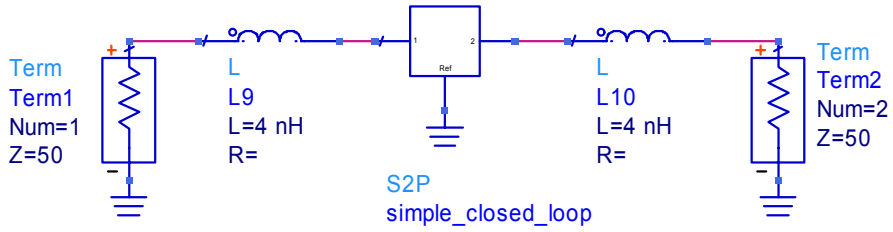

Figure 50: Circuit simulation of 3rd order Chebyshev filter using Square closed loop resonator with series inductors placed at each port to increase Q_L.

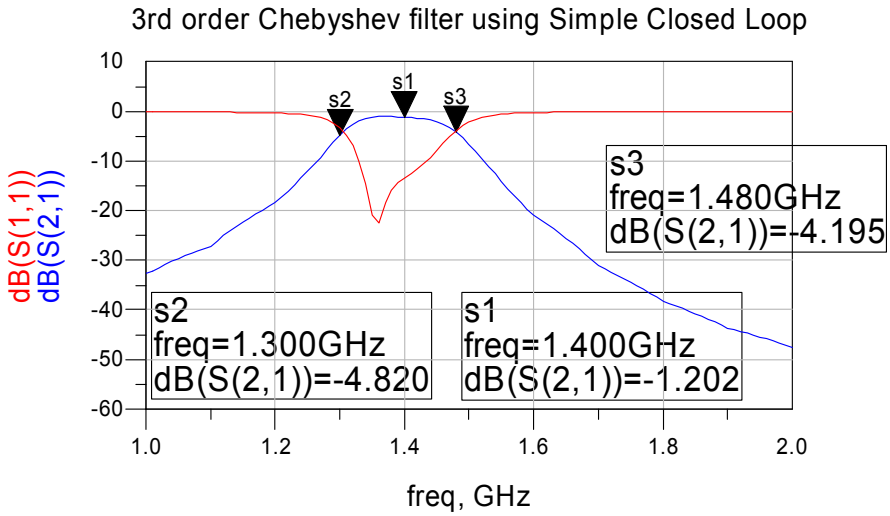

Simulated Response using IE3D & ADS circuit simulation

$F_0 = 1.4$ GHz ($|S21| = -1.47$ dB)

$F_{-3dB} = 1.3$ GHz ($|S21| = -4$ dB)

$F_{+3dB} = 1.48$ GHz ($|S21| = -4.4$ dB)

BW = 13%

Figure 51: Simulated response of the 3rd order filter using Square closed loop resonator

6.3 Chebyshev Filter of 0.01dB ripple, BW=10% Using Resonator dbl_d66.

The resonator dbl_d66 is determined in the previous chapters to have the following electrical characteristics:

Resonance Frequency: 1.08 GHz

Assuming a fabrication tolerance of gap ≥ 5 mils:

Coupling coefficient: $K \leq 0.09$

Q_L for tapped line coupling: $5.89 \leq Q_L \leq 36$

Q_L for coupled line coupling: $Q_L \geq 46.3$

The characteristics of resonator dbl_d66, enables filter of order N ≥3 to be synthesized. For ease of fabrication within in house facilities, a 3rd order filter is chosen to be made. The smaller overall area enables small gaps of 5mils on different parts of the structure to be fabricated and realized.

The K and Q values for N=3 are approximately translated to the following physical parameters based on the previously simulated results in Figure 41and Figure 48.

Coupling Coefficient K						Q-loaded	
N	**K12**	**K23**				**Qin**	**Qin**
3	0.128	0.128				6.292	6.292
Gap (mil)	5	5			**Feed structure**	5 stub	5 stub

Note: Gap of 5 mils rather than 3 mils is chosen for K_{12} & K_{23} to keep the design within fabrication tolerances.

The synthesized filter shown in Figure 52 occupies an area of 2058 in^2. Which is 38 in^2 smaller compared to the square loop resonator filter formed using resonators of equivalent overall size.

The simulated filter response shown in Figure 53 corresponds closely to desired result with bandwidth exceeding by only 1%.

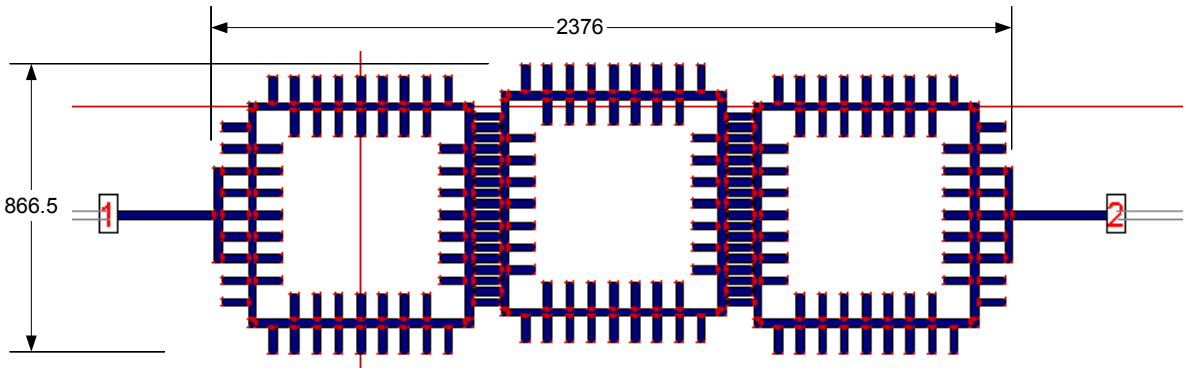

Figure 52: Layout of the 3rd Order Chebyshev filter using dbl_d66

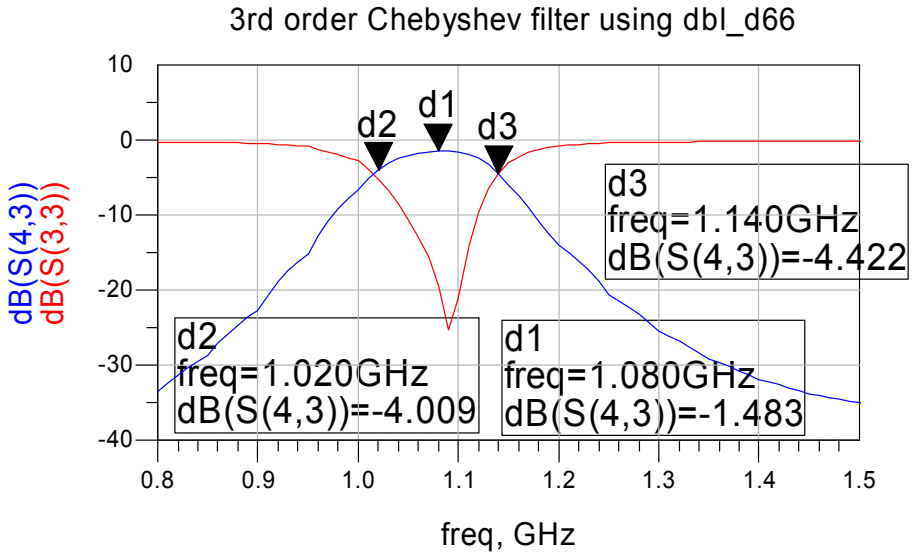

F_0 = 1.09 GHz (|S21| = -1.47 dB),

F_{-3dB} = 1.02 GHz (|S21| = -4 dB); F_{+3dB} = 1.14 GHz (|S21| = -4.4 dB)

BW = 11%

Figure 53: Simulated response (IE3D) of the 3rd order filter using dbl_d66

6.4 Fabricated and Measured Results

Illustrated in this section is the fabricated 3rd order Chebyshev filter using dbl_d66 and its measurement result. The results Figure 57 show that the measured response corresponds closely to the simulated response. Hence filter synthesis using resonator dbl_d66 has been successfully achieved.

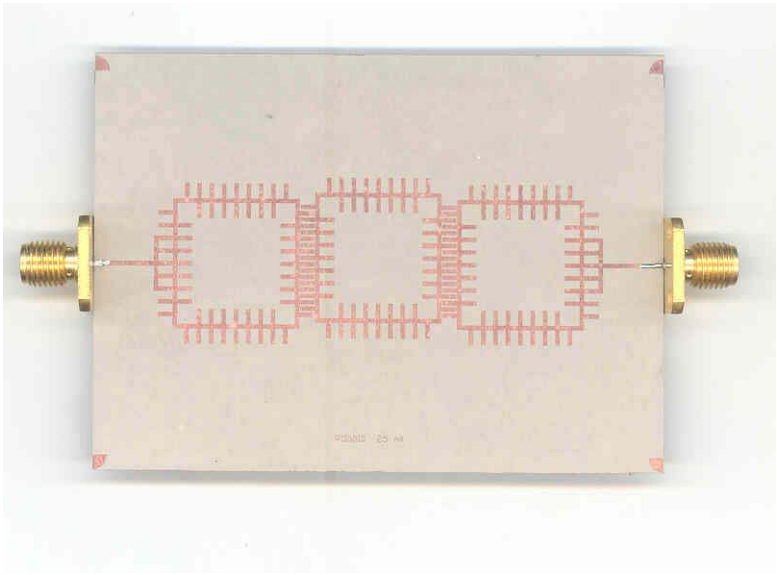

Figure 54: Fabricated 3rd order filter using dbl_d66

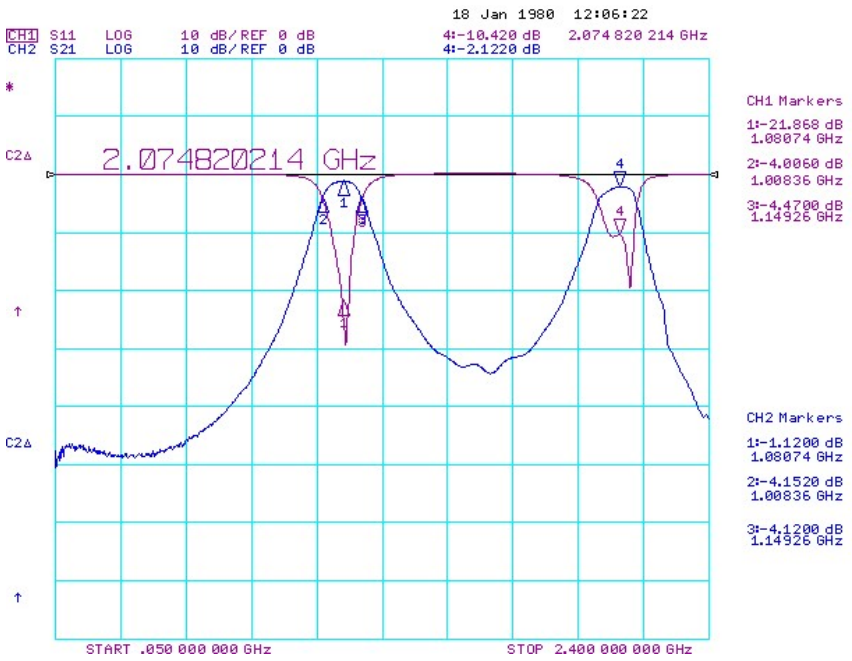

Figure 55: VNA measurement from 50 MHz to 2400 MHz

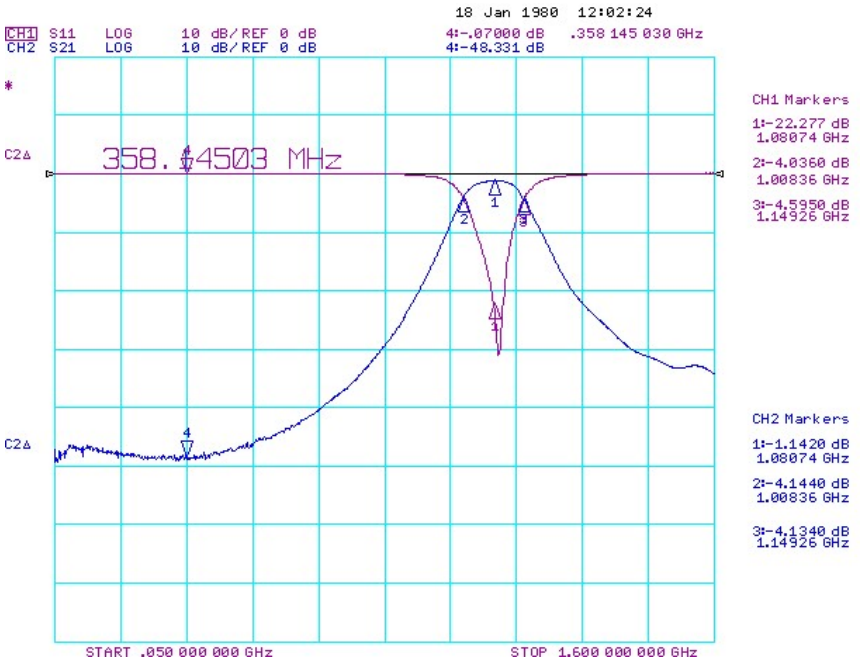

Figure 56: VNA measurement 50 MHz to 1600 MHz

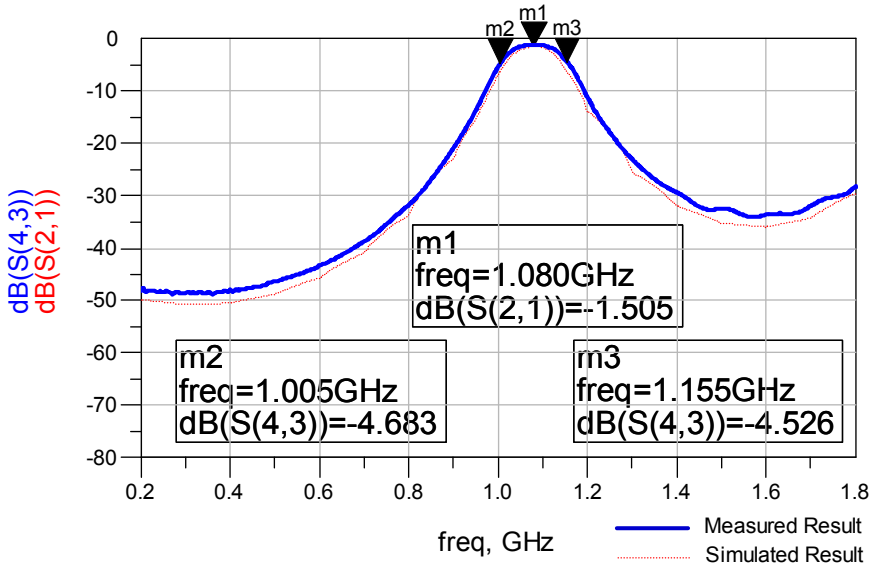

Figure 57: Compare simulated vs measured result

Measured Response:

F_0 = 1.08 GHz (|S21| = -1.12 dB)

F_{-3dB} = 1.01 GHz (|S21| = -4.15 dB)

F_{+3dB} = 1.15 GHz (|S21| = -4.12 dB)

BW = 13%

6.5 Summary

In this chapter filter synthesis using the miniaturized resonator has been successfully demonstrated. The measured result of the fabricated filter corresponds closely to the simulated results as shown in Figure 54.

Comparing the size and performance of a filter created using the simple closed loop resonator (Figure 53) against one created using the miniaturized resonator dbl_d66 (Figure 51), the following is observed:

- Filter using dbl_d66 occupies a slightly smaller area of 2.058 in^2 whereas the filter using the simple loop resonator occupies a slightly larger area of 2.096 in^2. This equates to approximately 6% reduction in area.
- Filter using dbl_d66 has a lower resonant frequency of 1.08 GHz as compared to 1.4 GHz. This equates to a 22% reduction in resonant frequency.

Chapter 7 : Conclusion

In this thesis, the objective of closed loop resonator miniaturization using capacitively loaded transmission lines (CTL) has been successfully achieved. The miniaturized resonator has been demonstrated to achieve 37% reduction in area over the square closed loop resonator of equivalent resonant frequency. A method to synthesize miniaturized closed loop resonators of the desired resonant frequency has been developed.

The miniaturized resonators offer improved coupling performance and control through the interdigital capacitor like structures that are formed when two resonators are placed adjacent to each other.

Planar feed structures to control the external Q_L of the miniaturized resonators have also been developed. The structures designed enable fine tuning of Q_L without the use of discrete lumped inductors.

Filter synthesis has successfully been performed on the newly developed structure. A 3rd order Chebyshev filter of 0.01dB ripple and 10% bandwidth has been fabricated and measured with simulation results corresponding closely to the measured results. In comparison to a filter synthesized using a closed loop resonator of similar size, the new structure achieves a 22% lower resonant frequency and also an area additional area reduction of 6% which is achieved due to the interdigital structure.

7.1 Suggestion for Future Works

In this thesis, the application of slow wave structures, in the form of capacitive open circuited microstrip line stubs to the closed loop resonator, has successfully enabled resonator miniaturization to be achieved.

For future studies, other forms of capacitive loading structures could be explored. This could be in form of lumped capacitors or other microstrip structures such as radial stubs.

Chapter 8 : Appendix

Parallel Coupled Line Feed

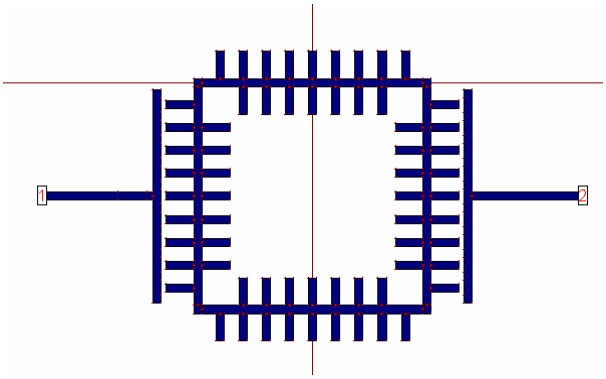

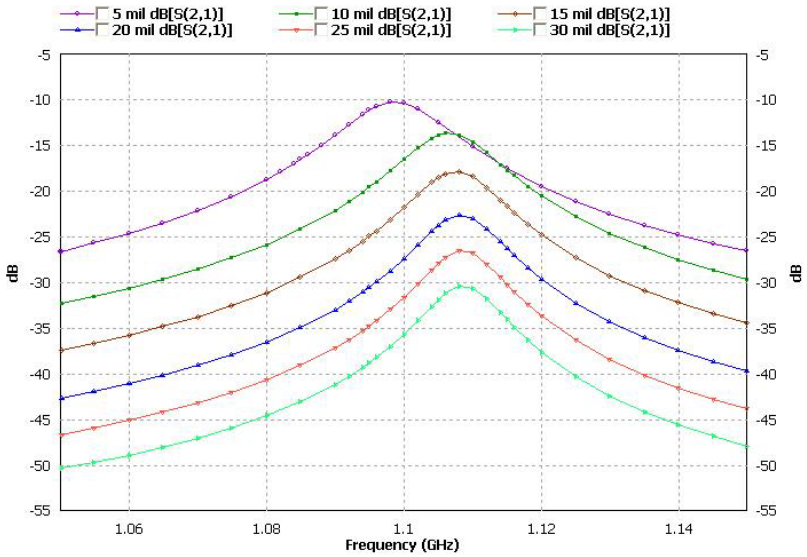

Feed gap (mil)	F1 (GHz)	F2 (GHz)	F0 (GHz)	Q-loaded
5	1.092	1.108	1.100	137.50
10	1.099	1.113	1.106	158.00
15	1.101	1.114	1.107	170.31
20	1.102	1.114	1.108	184.67
25	1.1026	1.114	1.108	194.39
30	1.103	1.114	1.108	201.42

Coupled Line with Interdigital stub feed

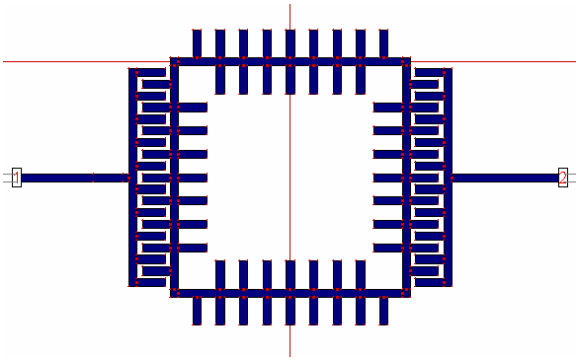

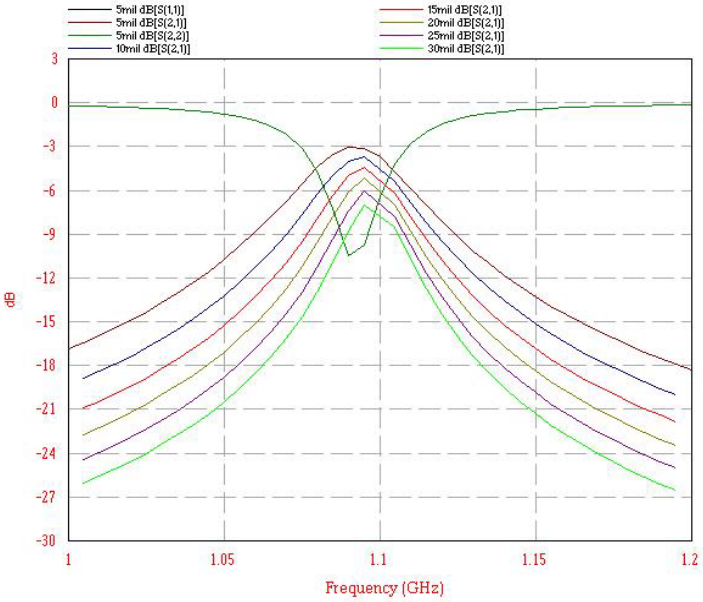

Reson sep (mil)	F1 (GHz)	F2 (GHz)	F0 (GHz)	Q-loaded
5	1.073	1.11	1.090	58.92
10	1.078	1.11	1.095	68.44
15	1.081	1.11	1.095	75.52
20	1.084	1.108	1.095	91.25
25	1.086	1.107	1.095	104.29
30	1.087	1.107	1.095	109.50

Coupled Line with X interdigital stubs (gap=15 mils)

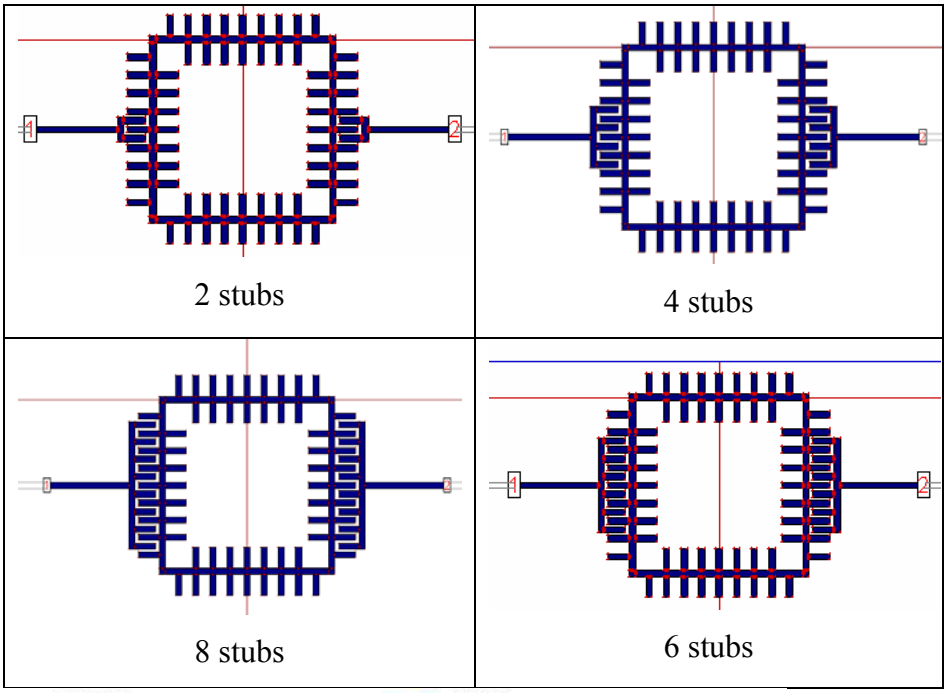

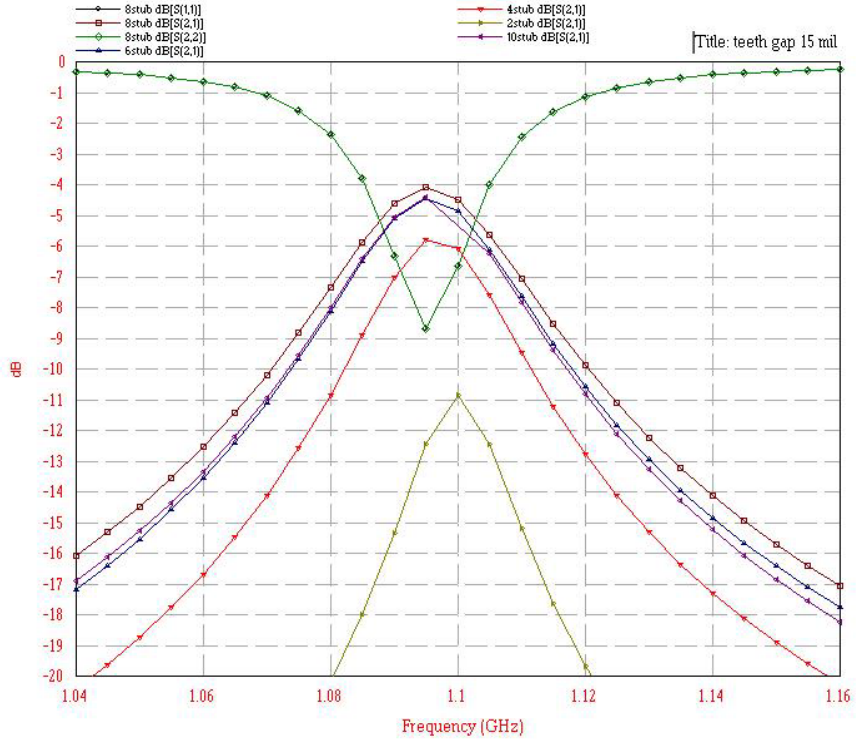

# of stubs	F1 (GHz)	F2 (GHz)	F0 (GHz)	Q-loaded
2	1.093	1.107	1.1	157.14
4	1.085	1.107	1.095	99.55
6	1.082	1.11	1.095	78.21
8	1.081	1.11	1.095	75.52
10	1.081	1.11	1.095	75.52

Tapped line coupled structures

Show S-parameter Plot beside each structure.

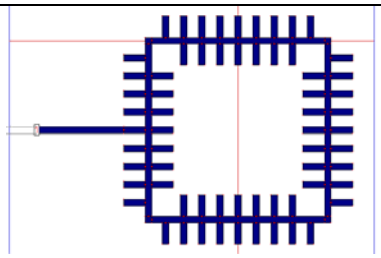 Center stub	
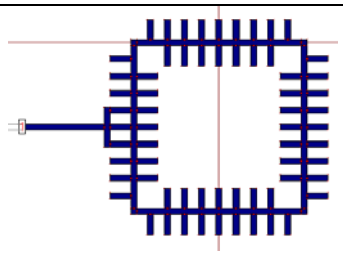 3 stubs	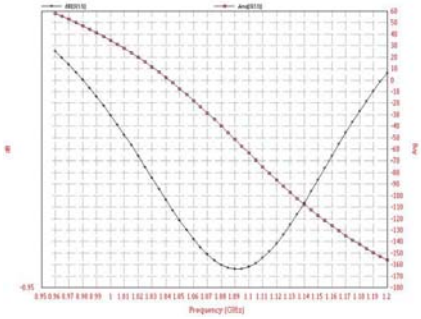
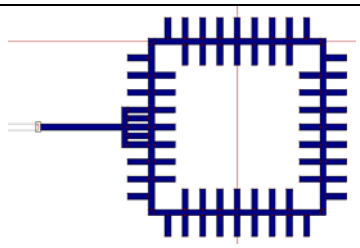 3 stubs + 2 pts	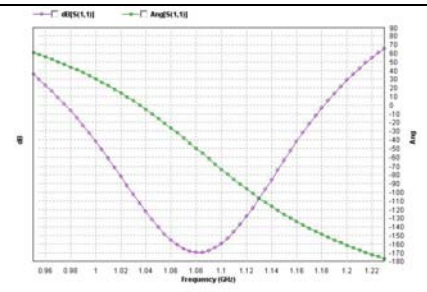
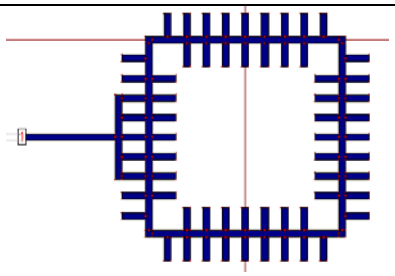 5 stubs	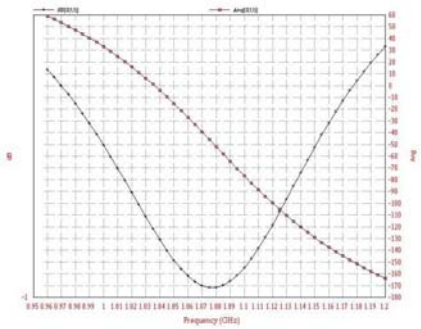
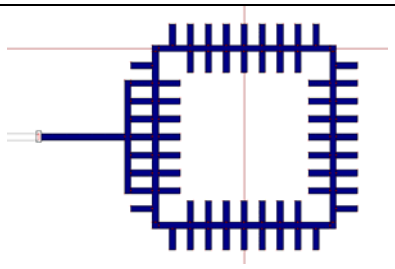 7 stubs	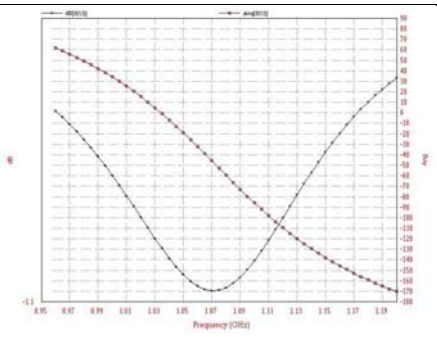

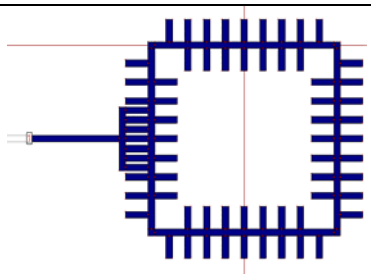 3 stubs + 4pts	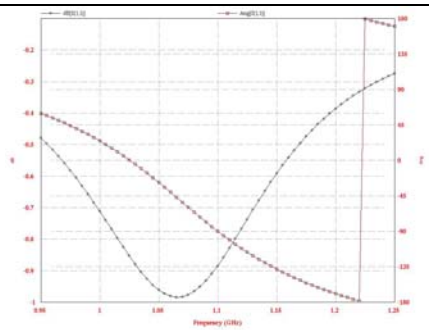
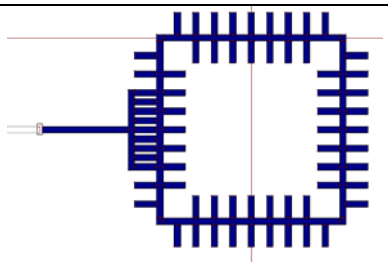 5 stubs + 4 pts	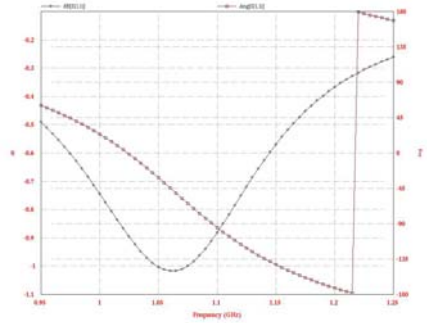
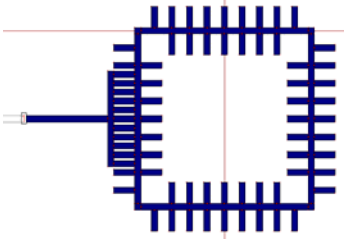 5 stubs + 6 pts	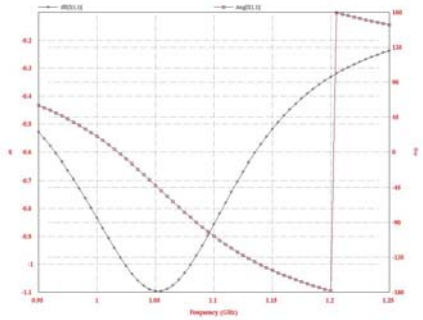
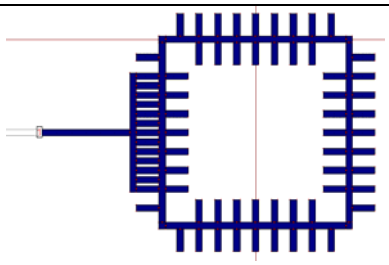 7 stubs + 6pt	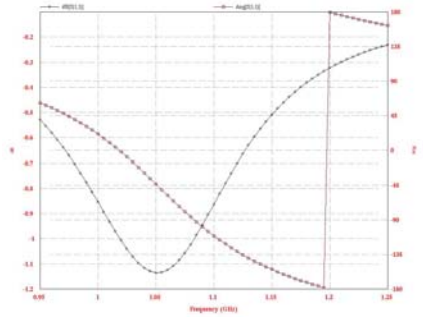
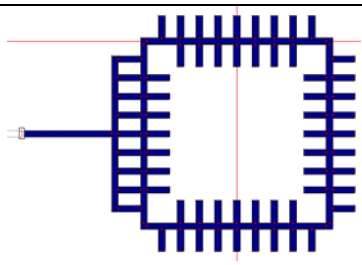 9 stubs	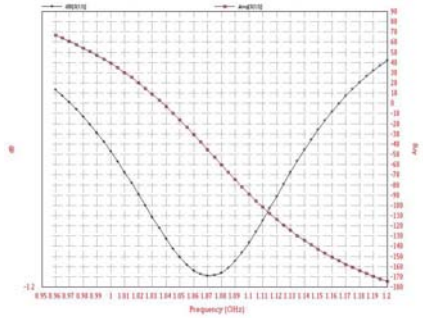

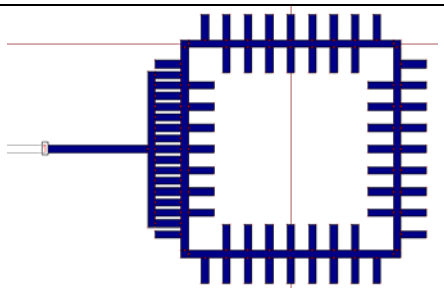

7 stubs + 8pts

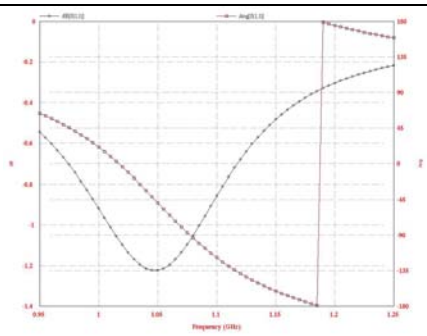

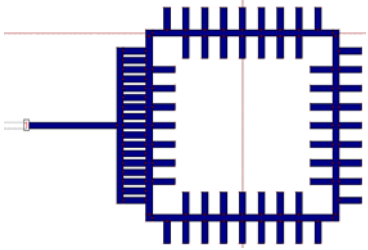

9 stubs + 8pts

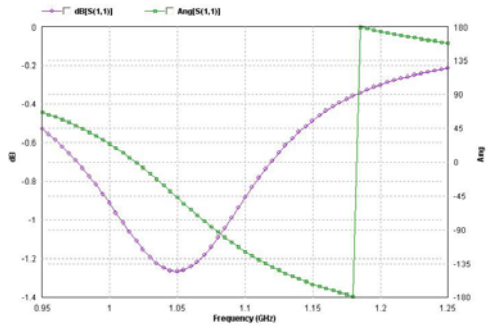

Feed	F+90 (GHz)	F-90 (GHz)	F0 (GHz)	Q-loaded
Center Stub	1.02	1.21	1.12	**5.89**
3 stubs	0.995	1.18	1.09	**5.89**
5 stubs	0.985	1.155	1.075	**6.32**
7 stubs	0.985	1.145	1.07	**6.69**
9 stubs	0.995	1.14	1.07	**7.38**
3stubs + 2pt	0.99	1.17	1.08	**6.00**
3stubs + 4pt	0.975	1.147	1.065	**6.19**
5stubs + 4pt	0.975	1.14	1.06	**6.42**
5stubs + 6pt	0.97	1.125	1.05	**6.77**
7stubs + 6pt	0.975	1.125	1.05	**7.00**
7stubs + 8pt	0.98	1.12	1.05	**7.50**
9stubs + 8pt	0.98	1.115	1.05	**7.78**

Coupling Measurement of Resonator dbl_d66

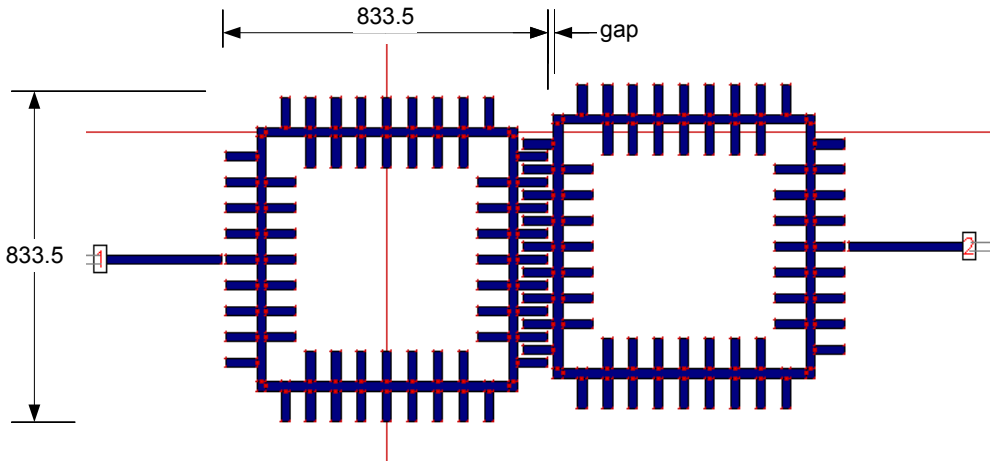

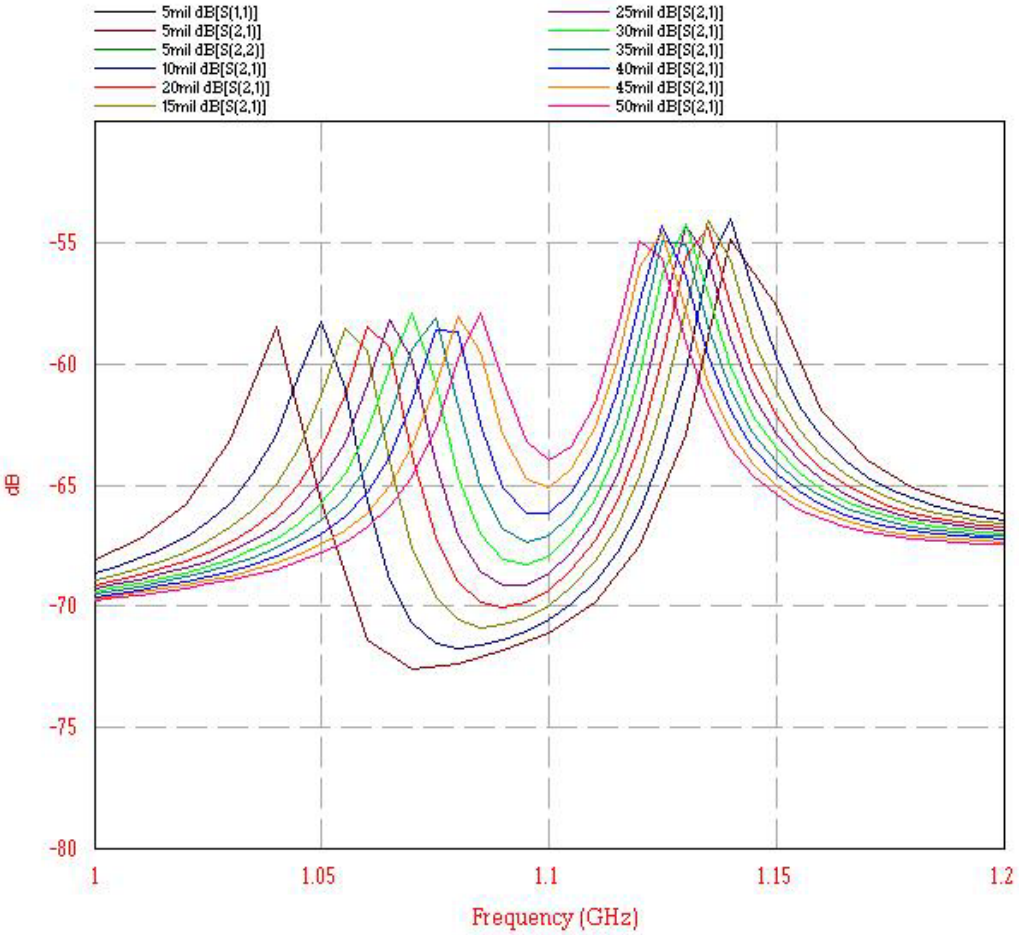

Reson gap (mil)	F1 (GHz)	F2 (GHz)	F0 (GHz)	k
3	1.04	1.15	1.094	0.10
5	1.04	1.14	1.089	0.09
10	1.05	1.14	1.094	0.08
15	1.055	1.135	1.094	0.073
20	1.06	1.135	1.097	0.068
25	1.065	1.13	1.097	0.059
30	1.07	1.13	1.100	0.055
35	1.075	1.135	1.105	0.054
40	1.077	1.125	1.101	0.044
45	1.08	1.125	1.102	0.041
50	1.085	1.12	1.102	0.032

Coupling Measurement of Square Closed Loop Resonator

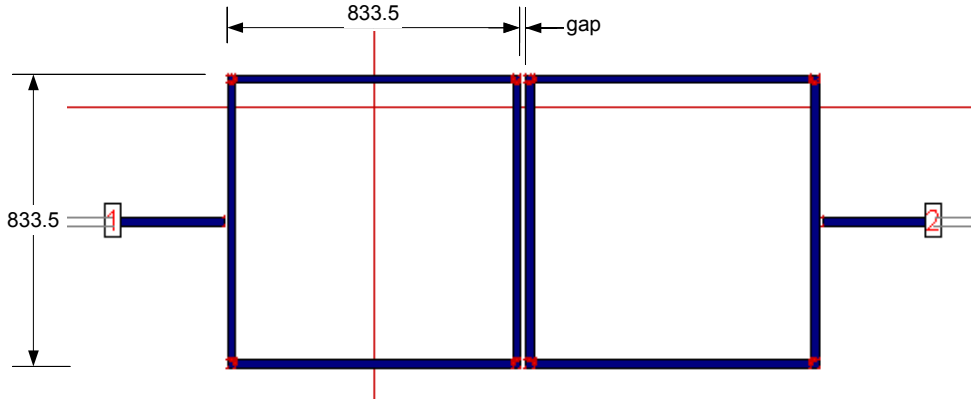

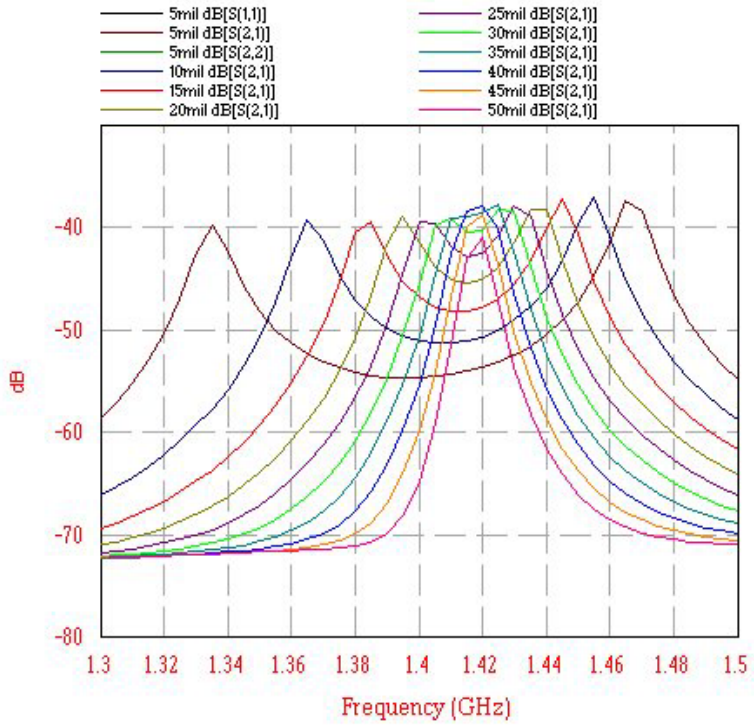

Reson sep (mil)	F1 (GHz)	F2 (GHz)	F0 (GHz)	k
5	1.335	1.465	1.398	0.09
10	1.365	1.455	1.409	0.06
15	1.385	1.445	1.415	0.042
20	1.395	1.44	1.417	0.032
25	1.4	1.43	1.415	0.021
30	1.41	1.425	1.417	0.011
35	1.42	-	1.42	coupling too weak
40	1.42	-	1.42	coupling too weak
45	1.42	-	1.42	coupling too weak
50	1.42	-	1.42	coupling too weak

References

[1] J.S. Hong and M.J. Lancaster, "Capacitively loaded microstrip loop resonator" *Electron. Lett,* vol. 30, no 18, pp1494-1495, Sept 1994

[2] A.gorur, C. Karpuz and M. alkan, "Characteristics of periodically loaded CPW structures" *IEEE Microwave Guided Wave Lett.,* vol.8, pp.278-280, Aug. 1998

[3] K.W Eccleston and H.M. Ong, "Compact Planar Microstripline Branch-Line and Rat-race Couplers" *IEEE Trans MTT* Vol 51, No 10, pp. 2119 – 2124, Oct 2003

[4] R.E. Collin, *Foundations for Microwave Engineering.* New York: Mc-Graw-Hill, 1992, ch 8.

[5] J.S. Hong and M.J. Lancaster, *Microwave filters for RF/Microwave applications*, Wiley, 2001.

[6] D.M. Pozar, *Microwave Engineering,* 2nd ed. New York: Wiley,1998.

[7] W.R Randall, *HF filter design and computer simulation*, Noble Publishing Associates, 1994

[8] A.B Williams and F.J Taylor, *Electronic Filter Design Handbook*, 2nd ed, McGraw-Hill, 1988

[9] Kai Chang, *Microwave Ring Circuits and Antennas*, Wiley-Interscience, 1996

[10] Bal S.Virdee, Christos Grassopoulosf', "*Folded Microstrip Resonator"* Microwave Symposium Digest, 2003 IEEE MTT-S International , Volume: 3 , 8-13 June 2003

[11] C.C Yu, Kai Chang, "Transmission-Line Analysis of a Capacitively Coupled Microstrip-Ring Resonator" IEEE Trans MTT, Volume: 45, No 11, pp. 2018-2024, Nov 1997.

[12] R.J Cameron, "*General Coupling Matrix Synthesis Methods for Chebyshev Filtering Functions*" IEEE Trans MTT, Volume: 47, No 4. pp. 1559–1564, Sep. 2000

[13] I.J. Bahl and P.Bhartia, *Microwave Solid State Circuit Design*, Wiley, 1988.

[14] G. Mattaei, L. Young, and E.M.T Jones, *Microwave Filters, Impedance matching networks, and coupling structures,* Artech House, 1980.

[15] K.C. Huang, D.Hyland, A.Jenkins "A miniaturized interdigital microstrip bandpass filter" IEEE Trans on Applied Superconductivity, Vol.9, no.2, pp.3889-3892 ,June 1999.

[16] D.Ahn, J.S. Lim, I.S. Kim "Design of a 2-pole bandpass filter using closed loop resonator and coupled lines" IEEE MTT-S digest, pp. 1643-1646, 1996.

[17] K.Y Kang, S.K. Hang “HTS 4 pole bandpass filter with closed loop resonators and coupled lines using YBCO thin films for PCS” Asia Pac Microwave Conference, pp. 105-108, 1997.

[18] D.Ahn, J.S. Lim, I.S. Kim “The design of closed loop type BPF with two attenuation poles at the upper side of passband” Asia Pac Microwave Conference, pp. 821-824, 1997.

[19] L.Zhu and K.Wu “A general purpose circuit model of interdigital capacitor for accurate design of low-loss microstrip circuit” IEEE MTT-S digest, pp. 1755-1758, 1998

[20] G.D. Alley “ Interdigital Capacitors and their application to lumped-element microwave integrated circuits” IEEE Trans MTT, Vol: 18, No 4, pp.1028-1033, Dec 1970.

[21] J.S.Hong, M.J. Lancaster “Microstrip slow-wave open-loop resonator filters” IEEE MTT-S digest, pp. 713-716 ,1997

[22] ADS2002, Agilent

[23] Zeland Software Inc., IE3D simulator